Author Manuscript
Faculty of Biology and Medicine Publication

Published in final edited form as:

serval
serveur académique lausannois

UNIL | Université de Lausanne
Faculté de biologie
et de médecine

Title: Synaptic Integration of Adult-Born Hippocampal Neurons is Locally Controlled by Astrocytes

Authors: Sébastien Sultan[1], Liyi Li[2], Jonathan Moss[1], Francesco Petrelli[1], Frédéric Cassé[1], Elias Gebara[1], Jan Lopatar[1], Frank W. Pfrieger[3], Paola Bezzi[1], Josef Bischofberger[2], Nicolas Toni[1]#

Affiliations:

1: University of Lausanne, Department of Fundamental Neurosciences, 9 rue du Bugnon, 1005 Lausanne, Switzerland

2: Department of Biomedicine, Physiological Institute, University of Basel, Pestalozzistrasse 20, 4056 Basel, Switzerland.

3: CNRS UPR 3212, University of Strasbourg, Institute of Cellular and Integrative Neurosciences, 67084 Strasbourg, France

#Contact information: Nicolas Toni, University of Lausanne, Department of Fundamental Neurosciences, 9 rue du Bugnon, 1005 Lausanne. Phone: +4121-692-5133. Email: Nicolas.toni@unil.ch

SUMMARY

Adult neurogenesis is regulated by the neurogenic niche, through mechanisms that remain poorly-defined. Here, we investigated whether niche-constituting astrocytes influence the maturation of adult-born hippocampal neurons using two independent transgenic approaches to block vesicular release from astrocytes. In these models, adult-born neurons but not mature neurons showed reduced glutamatergic synaptic input and dendritic spine density that was accompanied with lower functional integration and cell survival. By taking advantage of the mosaic expression of transgenes in astrocytes, we found that spine density was reduced exclusively in segments intersecting blocked astrocytes, revealing an extrinsic, local control of spine formation. Defects in NMDA-receptor mediated synaptic transmission and dendrite maturation were partially restored by exogenous D-serine, whose extracellular level was decreased in transgenic models. Together, these results reveal a critical role for adult astrocytes in local dendritic spine maturation, which is necessary for the NMDAr-dependent functional integration of newborn neurons.

INTRODUCTION

Adult neurogenesis occurs in the brains of most mammals (Altman and Das, 1965) including humans (Eriksson et al., 1998), and contributes to learning and memory (Aimone and Gage, 2011; Zhao et al., 2008). The survival and synaptic integration of adult-born hippocampal neurons is enhanced by neuronal network activity or the induction of long-term potentiation (LTP), a physiological mechanism of synaptic plasticity (Bruel-Jungerman et al., 2006). In turn, the incorporation of adult-born neurons with increased synaptic plasticity (Ge et al., 2007; Schmidt-Hieber et al., 2004) enhances LTP and hippocampal-dependent learning performances (Kempermann and Gage, 1999). Adult neurogenesis is highly regulated and a growing number of studies indicate that the direct cellular environment of adult neural stem cells, the neurogenic niche, provides pro-neurogenic cues (Song et al., 2002). A major component of the neurogenic niche is the astroglia, which release soluble molecules that control distinct steps of adult neurogenesis, including the proliferation of the stem cells (Cao et al., 2013), their differentiation into neuronal lineage (Song et al., 2002) and their survival

(Platel et al., 2010). Here, we examined whether astrocytes regulate the synaptic integration of adult-born neurons, a major step of adult neurogenesis.

Previous studies have shown that during development, astrocytes promote the formation of synapses in distinct neuronal populations (Allen, 2013). Indeed, soluble molecules contained in astrocyte-conditioned medium induce the formation of synapses on early postnatal retinal ganglion cells (Banker, 1980; Pfrieger and Barres, 1997). These molecules display a great diversity of class, ranging from protein components of the extracellular matrix, such as thrombospondin to membrane lipids such as cholesterol (Christopherson et al., 2005; Mauch et al., 2001). They also express a variety of properties, since some astrocyte-secreted molecules such thrombospondins induce the formation of structurally mature but functionally silent synapses because of a lack of AMPA receptors (Christopherson et al., 2005), whereas others molecules such as Glypicans are involved in the functional maturation of synapses by facilitating the insertion of AMPA receptors in the postsynaptic membrane (Allen et al., 2012). However, the formation of synapses on adult-born neurons differ from developmental synaptogenesis on two major aspects: First, during perinatal development, pre- and postsynaptic neurons mature concomitantly and newly formed dendritic spines contact immature axon terminals. In the adult hippocampus in contrast, new spines preferentially contact pre-existing, functionally mature axon terminals which already synapse with other dendritic spines, thereby forming multiple-synapse boutons, where two or more postsynaptic neurons contact the same axonal terminal (Toni et al., 2007) (Figure S1A). Over time, multiple-synapse boutons transform into single-synapse boutons (Toni et al., 2007), suggesting that new spines replace more mature spines through a competitive process occurring between immature and mature neurons (Toni and Sultan, 2011). This process may play a role in the integration of new neurons into the adult neuronal network and regulate the functional implication of new neurons on the hippocampus (Bergami and Berninger, 2012; Tashiro et al., 2006). Furthermore, the synaptic integration of new neurons is strongly activity-dependent. Indeed, during an early developmental stage, new neurons express NMDAr, but not AMPAr-mediated glutamatergic synaptic transmission and are therefore functionally silent. At this stage, GABAa receptor-mediated depolarization enables NMDAr activation, the expression of AMPA receptors and synapse unsilencing, a mechanism that is also induced by exposure to an enriched environment (Chancey et al., 2013). Interfering with GABAa-mediated depolarization results in impaired dendritic development and synaptic integration (Ge et al., 2006). Similarly, the cell-specific knock-out of the essential NR1 subunit of the NMDA receptor drastically reduces the synaptic integration and survival of new

neurons (Tashiro et al., 2006), which can be partially rescued by reducing overall NMDA receptor activity with injections of the specific antagonist CPP during a critical phase of maturation (Tashiro et al., 2007; Tashiro et al., 2006). Together, these studies indicate that the integration of new neurons depends on neuronal network activity and an activity-dependent competitive process between immature and mature neurons. Second, developmental synaptogenesis occurs in the presence of highly proliferative, immature astrocytes, which release pro-synaptogenic molecules (Allen, 2013; Allen et al., 2012; Christopherson et al., 2005; Pfrieger and Barres, 1997). In contrast, in the adult brain, the generation of glia is drastically reduced (Ge et al., 2012) and as a consequence, newborn neurons are principally in contact with mature, pre-existing astrocytes (Krzisch et al., 2014). Furthermore, the reduction in astrocytic signaling with age (Okamoto et al., 2011; Sun et al., 2013) suggests that mature astrocytes may be less amenable to synaptogenesis than immature astrocytes. It is therefore unclear to which extent adult astrocytes may contribute to synaptogenesis and play a role in this late phase of adult neurogenesis.

In the current study, we examined the role of exocytosis from astrocytes on the synaptic integration of adult-born hippocampal neurons. We used two distinct conditional transgenic mice to manipulate exocytosis from astrocytes during the maturation stage of new neurons identified and birth-dated by viral-mediated gene transfer (Figure S1B). We found that blocking vesicular release from astrocytes resulted in impaired dendritic maturation of new neurons: dendrites were shorter and less branched, bore fewer dendritic protrusions with an immature morphology. This effect was specific for adult-born neurons and restricted to the territories of impaired astrocytes, revealing a local regulation of synapse formation within specific dendritic segments newborn neurons. These impairments were accompanied by a reduced extracellular D-serine concentration and reduced NMDAr currents which were alleviated by application of the co-agonist D-serine. Finally, we found that the chronic administration of D-serine restored the dendritic development of new neurons in the absence of astrocytic vesicular release. Together, these results indicate that D-serine released by astrocytes is required for the NMDAr-dependent maturation, synaptic integration and survival of adult-born hippocampal neurons. These results underline the fundamental role of astrocytes in the regulation of adult brain plasticity.

RESULTS

Inducible inhibition of vesicular release in astrocytes

To investigate the role of astrocytes on the maturation of adult-born hippocampal neurons, we used two complementary mouse models enabling the control of SNARE-dependent exocytosis in astrocytes. The first model, the iBot-Glast-CreER^{T2} mouse line, enables the tamoxifen-inducible, stable expression of the *Clostridium botulinum* toxin serotype B light chain (boNT/B) and the enhanced green fluorescent protein (GFP) in astrocytes (Figure 1A-B, Figure S2A-C). boNT/B cleaves the vesicle-associated membrane synaptobrevin-2, a component of the SNARE complex, resulting in impaired vesicular release (Schiavo et al., 1992; Slezak et al., 2012). The second mouse model, the dnSNARE mouse line, expresses the dominant-negative SNARE domain of the synaptobrevin-2 protein and GFP in astrocytes under the control of a tet-off tetracycline transactivator system controlled by doxycycline (Dox; Figure S2D-G) (Pascual et al., 2005). To directly assess the effect of this construct on vesicular release, we examined exocytosis *in vitro* on hippocampal astrocytes using total internal reflection fluorescence (TIRF) microscopy. When compared to wild-type (WT), astrocytes from dnSNARE mice showed a 91% reduction in the number of fusion events (Figure S2H-J). Thus, interfering with synaptobrevin-2 function in astrocytes resulted in a drastic reduction of vesicular fusion.

Inhibition of astrocytic SNARE-mediated release locally impairs the dendritic maturation and survival of adult-born neurons.

We then assessed the maturation of adult-born neurons in mice expressing boNT/B or dnSNARE in astrocytes. Newly-formed cells were identified using injections of either the cell proliferation tracer 5-Bromo-2-deoxyuridine (BrdU), or an engineered Moloney murine leukemia virus encoding for the red fluorescent protein (RFP) in dividing cells (see supplemental procedures). In each mouse line, we labeled newly-formed cells before the induction of transgene expression in astrocytes: For the iBot mouse line, new neurons were labeled 7-8 days before tamoxifen injections (Figure 1C) and for the dnSNARE mouse line, Dox was withdrawn immediately after the labeling of new neurons (Figure 2A). The neuronal progenies were analyzed 30 days post-injection (dpi). Therefore, the labeled neural progenitors could proliferate in absence of transgene expression whereas their progenies, newly-formed neurons, matured in the presence of astrocytes expressing the respective transgenes. Also, since adult neural stem cells express GLAST and GFAP (Kronenberg et al.,

2003), this specific experimental design was important to avoid transfer of transgene expression in the labeled new neurons. Consistently, immunostaining against GFP followed by both confocal microscopy and electron microscopy (EM) in the molecular layer and the granule cell layer of the dentate gyrus (DG) revealed a strong expression of GFP in astrocytes but not in neurons or other cell types (Figure S2 B-C and S3). Notably, $35 \pm 12\%$ (n=5 mice) of GFAP-immunostained astrocytes co-expressed GFP in iBot-Glast-CreER^{T2} Tam-injected mice (Figure 1A-B) and $49.9 \pm 1.3\%$ in dnSNARE mice (n=5 mice) (Figure S7 A-D) indicating a mosaic expression of transgenes. Therefore, astrocytes not expressing the transgenes could be used as internal controls. Since astrocytes occupy distinct, non-overlapping territories (Bushong et al., 2004; Bushong et al., 2002) and the dendrites of any given adult-born neuron crossed the territories of both transgene-expressing astrocytes and normal astrocytes, we assessed whether the locally confined presence of the transgene affected protrusions along a given dendrite. Remarkably, dendritic protrusion density and protrusion head diameter were significantly reduced in the dendritic segments that crossed transgene-expressing astrocytes in both iBot-Glast-CreER^{T2} Tam-injected mice (Figure 1D-F) and dnSNARE mice (Figure 2B-G). In contrast, segments of the same neurons that extended outside of transgene-expressing astrocytic territories displayed comparable spine density to new neurons generated in control littermate mice (bilateral t-test P>0.05 for iBot-Glast-CreER^{T2} Tam-injected mice, ANOVA F(2.14)=3.34; P>0.05 for dnSNARE animals). The reduction of protrusion density and maturation observed in both mice was not due to GFP expression in astrocytes, since new neurons formed in GFAP-GFP transgenic mice, which lack dnSNARE or boNT/B expression, showed homogenous protrusion density along their dendrites (Figure S4). Therefore, the dendrites of new neurons displayed reduced spine density and spine maturation exclusively in segments that crossed transgene-expressing astrocytes and this reduction followed the shape of transgene-expressing astrocytes' territories (Figure 2E). This observation indicates that astrocytes locally control spine density in specific segments of the growing dendritic tree.

We next examined whether the sum of local reductions in dendritic spine density resulted in reduction of global spine density on new neurons. In dnSNARE animals, individual neurons intersected with the territories of several transgene-expressing astrocytes, averaging $38.3 \pm 1.7\%$ of the total length of their dendritic arbor (n=50 neurons, range: 17 to 67%). Since spine density was 0.49 spines/µm in these territories (Figure 2F) and spine density on adult-born neurons in WT mice averaged 1.12 spines/µm (Figure 2I), the predicted total spine density on entire newborn neurons in dnSNARE mice was expected to drop to 0.87

spines/µm, which is remarkably similar to the measured total spine density (0.81 ± 0.1 spines/µm, Figure 2I). Similarly, global spine morphological maturation was impaired on new neurons in dnSNARE mice (Figure 2J). Furthermore, the reduction in total dendritic protrusion density on individual neurons was correlated with the proportion of their dendritic arbor covered by transgene-expressing astrocytes (Figure 2H). Similar observations were done in iBot-Glast-CreER^{T2} Tam-injected mice: the global density of dendritic protrusions and the proportion of protrusions with a mature morphology were reduced compared to control, tam-injected animals and control animals injected with vehicle (No Tam, Figure 1G-I). Together, these results indicate that blocking astrocyte exocytosis induced local reductions of spine density and maturation, which resulted in reduction of total spine density on new neurons.

Next, we examined dendritic development of new neurons using Scholl analysis. In dnSNARE mice, the dendritic arborization of individual neurons was decreased as compared to wild-type or single transgenic mice (Figure 2K-L). Dendritic length was also decreased and was inversely correlated with the proportion of their arbor that intersected transgene-expressing astrocytes (Figure 2M-N), consistently with the observation that the sum of local impairments of dendritic maturation reduced global maturation of new neurons. In iBot-Glast-CreER^{T2} Tam-injected mice, the dendritic length of newborn neurons but not their arborization was also reduced (Figure 1J-L). Thus, blocking vesicular release from astrocytes reduced the dendritic maturation of new neurons.

The survival of adult-born neurons depends on their synaptic integration during a critical period (Tashiro et al., 2007; Tashiro et al., 2006). We therefore examined whether the reduction of dendritic maturation on newborn neurons in dnSNARE mice was accompanied by alterations in their survival. Mice were injected with BrdU and Dox was withdrawn shortly thereafter. The number of newly divided cells was analyzed by immunohistochemistry 1 day later (Figure 2O). The number of BrdU$^+$ cells was not different between dnSNARE and control mice (Figure 2P-Q), indicating that cell proliferation was not altered shortly after Dox withdrawal, consistently with a latency in transgene expression after Dox withdrawal (Figure S2F-G). When mice were analyzed two weeks after BrdU injections and Dox removal, no difference in BrdU+ cells density was observed between dnSNARE and WT mice (data not shown, bilateral t-test P>0.05). In contrast, when BrdU immunostaining was assessed one month after injection and doxycycline removal, cells that divided before Dox removal but matured after transgene expression showed a 40% decrease in survival in dnSNARE compared to WT mice (Figure 2R). Similar observations were found with the iBot mouse line

(Figure 1M). Thus, the impaired dendritic maturation was accompanied with reduced survival of new neurons.

dnSNARE expression in astrocytes reduces the synaptic integration of new neurons

To assess whether dendritic protrusions from adult-born neurons formed mature synapses with presynaptic boutons, new neurons were identified with a GFP-encoding virus, followed by serial section immuno-EM. Within the territories of dnSNARE transgene-expressing astrocytes as well as in territories of astrocytes not expressing the transgenes, all the observed dendritic spines from new neurons formed synapses, defined by the presence of presynaptic vesicles accumulation, a widening of the synaptic cleft, cleft material and a postsynaptic density (Figure 3A-C). Furthermore, the proportion of spines forming multiple synapse boutons (MSB) was similar between territories in mature neurons (GFP⁻ spines; 42.3 % in territories of transgene-expressing astrocytes, 46.1% outside transgene-expressing territories), as well as in newborn neurons (73% vs. 71% respectively, data not shown), consistent with previous observations (Toni et al., 2007). However, consistent with confocal microscopy observations, the protrusion head volume on newborn neurons was significantly smaller in dendritic segment within the territory of transgene-expressing astrocyte than in dendritic segments outside these territories or in WT mice (nonparametric Wilcoxon test, P=0.003, data not shown).

Direct contact with astrocytes regulates the stabilization and maturation of dendritic spines (Nishida and Okabe, 2007). To examine whether dnSNARE expression in astrocytes may interfere with the fine structure of their processes and the contact they establish with new neurons, we examined the proportion of surface area of synapses that was ensheathed by astrocytes. On both GFP⁺ newborn neurons and GFP⁻ neurons, transgene-expressing astrocytes ensheathed the same proportion of synaptic surface area as astrocytes not expressing the transgene and wild-type astrocytes (Figure 3 D-E). This indicates that the effect of dnSNARE-expressing astrocytes on new neurons' maturation was due to impaired astrocytic function and not to impaired structural integrity.

We next assessed the functional integration of newborn neurons in dnSNARE mice. Impaired dendritic maturation may interfere with the functional integration of adult-born neurons and result in functional deficits of excitatory synaptic transmission. Since AMPA receptors are absent from filopodia and their density correlates with dendritic protrusion head diameter (Matsuzaki et al., 2001; Takumi et al., 1999), the combination of decreased dendritic

protrusion head diameter (15%, data not shown), decreased dendritic protrusion density (28%, Figure 2I) and decreased dendritic length (28%, Figure 2M) observed on adult-born neurons in dnSNARE mice may result in an overall reduction of glutamatergic synaptic input. To assess synaptic transmission in newborn neurons, we performed whole-cell patch clamp recordings in acute brain slices from adult WT or dnSNARE mice and measured synaptic currents in response to extracellular perforant-path stimulation. Adult-born neurons in dnSNARE mice, as compared to WT mice, displayed a significant reduction of AMPA-receptor mediated excitatory postsynaptic currents (EPSCs) by about 70% (Figure 4A-B). NMDA receptor-mediated EPSCs were also significantly reduced, but less so than AMPAr EPSCs, resulting in a two-times larger NMDA EPSC/AMPA EPSC ratio (Figure 4 C-D). The reduced amplitude of evoked synaptic currents suggests that the young neurons might have formed fewer excitatory synapses. To assess the number of functional synaptic release sites, we recorded miniature EPSCs (mEPSCs) in the presence of TTX. Newborn neurons in dnSNARE mice showed reduced frequency and amplitude of mEPSCs, without changes in mEPSC decay time course, consistent with a lower dendritic spine density and a higher proportion of immature synapses (Chancey et al., 2014; Schmidt-Salzmann et al., 2014), (Figure 4E-J). Altogether, morphological and electrophysiological data converge to the conclusion that inhibition of exocytosis in astrocytes reduces the number and size of functionally mature synapses in newborn neurons.

dnSNARE expression in astrocytes does not interfere with the stability of mature synapses, nor with synapses on mature neurons

To examine whether the reduced dendritic maturation of newborn neurons was transient, we examined them at 21 and 90 dpi (Figures S5 and S6, respectively). Similar to 30 dpi, dendritic protrusion density and diameter in segments intersecting transgene-expressing astrocytes was reduced at 21 and 90 dpi in dnSNARE as compared to WT mice, indicating that astrocytic impairment resulted in early-onset and long-lasting maturation defects in newborn neurons. Furthermore, the survival of $BrdU^+$/$NeuN^+$ new neurons in dnSNARE mice was reduced by 20% at 21 dpi, 43% at 30 dpi (Figure 2R) and 45% at 90 dpi, indicating that astrocytic vesicular release was particularly important for the survival of new neurons during the entire period of excitatory synapse formation.

The observed reduction in spine density may be due to impaired dendritic spine formation, impaired stabilization, or both. To test these possibilities, we first assessed whether spines formed prior to transgene expression may be destabilized upon impaired astrocytic function.

To this aim, dnSNARE expression was induced by removing Dox 30 days after viral infection, a time point when new neurons have already formed most dendritic protrusions (Toni et al., 2007) and neuronal morphology was analyzed immediately (i.e. at 30 dpi) and 30 days later (60 dpi.). At 30 dpi, spine density was similar between WT and dnSNARE mice (Figure 5A-B), indicating that spine formation was not altered upon transgene repression by Dox. At 60 dpi however, the density and maturation of dendritic protrusions of adult-born neurons was slightly but significantly decreased in dnSNARE compared to WT mice and this reduction was observed only in dendritic segments intersecting transgene-expressing astrocytes (Figure 5B-E). However, in both mice, protrusions density at 60 dpi was greater than at 30 dpi (bilateral t-test p<0.05), suggesting that blocking vesicular release from astrocytes did not prune dendritic protrusions formed prior to the induction, but reduced the formation of new protrusions.

Next, we tested whether dendritic protrusions from mature neurons may be affected by impaired astrocytic function. Thirty days after Dox removal, random dendrites (i.e. principally from mature granule neurons) of dnSNARE and WT mice were fluorescently labeled using the application of the lipophilic dye DiI in the molecular layer. In contrast to newly-generated adult-born neurons, we found no difference in dendritic protrusion density in mature neurons between groups of mice and between dendritic segments inside and outside territories of transgene-expressing astrocytes (Figure 5F-I).

Similarly, GFP$^-$ synapse density (i.e. synapses from random neurons) measured by serial section EM and unbiased stereology, was similar between territories of transgene-expressing astrocytes and the territories of astrocytes not expressing the transgene (Total of synapses analyzed: 696; t-test, P>0.05, data not shown). Furthermore, serial-section EM and 3D reconstructions of GFP$^-$ spines inside and outside the territories of transgene-expressing astrocytes had similar spine head volume as in WT mice (total number of spines analyzed: 46; Kruskal Wallis, P=0.1134, data not shown).

These results indicate that dnSNARE expression in astrocytes did not interfere with the stability or the morphology of pre-established synapses from both mature and adult-born neurons. Thus, the reduction in dendritic protrusion density in the territories of transgene-expressing astrocytes was specific to new neurons.

D-serine mediates the astrocyte-dependent synaptic integration of adult-born neurons

Finally, we assessed the mechanisms involved in the regulation of astrocyte-dependent synaptic integration of adult-born neurons. During their development, adult-born neurons

transition through a silent stage, during which glutamatergic transmission is mediated by NMDA receptors only. During this period, the pairing of GABA-mediated depolarization and synaptic stimulation enables the activity-dependent expression of AMPA receptors and synapse unsilencing (Chancey et al., 2014), whereas the knock-down of the essential NR1 subunit of the NMDA receptor results in the drastic elimination of new neurons (Tashiro et al., 2006). Astrocytes release several molecules known to target neurotransmitter receptors (Araque et al., 2014). We therefore examined whether dnSNARE expression in astrocytes affected the extracellular level of agonists of glutamatergic and GABAergic receptors, namely D-serine, Glycine, Glutamate and GABA, using microdialysis in the DG followed by HPLC. One month after Dox removal, no difference was observed in the extracellular concentrations of Glutamate, Glycine and GABA in the DG of dnSNARE mice as compared to WT animals. In contrast, the extracellular concentration of D-serine was significantly decreased in dnSNARE mice (Figure 6A-B). D-serine is a NMDA receptor co-agonist, known to be released by astrocytes in a SNARE-dependent manner (Fellin et al., 2009; Henneberger et al., 2010; Martineau et al., 2013). However, D-serine can also be synthesized and released by neurons (Kartvelishvily et al., 2006). To directly assess the astrocytic release of D-serine, we analyzed the concentration of D-serine in a buffered saline solution (HEPES Tyrode's solution) conditioned by purified hippocampal astrocytes. Consistent with our *in vivo* observations, D-serine concentration was significantly reduced in medium conditioned by dnSNARE-expressing astrocytes as compared to medium conditioned by WT astrocytes (Figure 6C-E). This effect was not due to difference in culture conditions, since protein content was similar between groups (Figure 6D). These results indicate that blocking astrocytic exocytosis was accompanied by a reduction of extracellular D-serine in the DG of dnSNARE mice.

The reduced extracellular D-serine concentration in dnSNARE mice may underlie the reduced NMDAr EPSCs observed in new neurons. To test this possibility, we measured the effect of exogenous D-serine application on synaptic NMDAr EPSCs in newborn neurons in acute brain slices from adult mice at 30 dpi. D-serine (50 μM) significantly increased NMDA EPSCs in newborn neurons in dnSNARE mice, but not in WT mice (Figure 6F-H).

Finally, to test the possibility that neuronal impairment in dnSNARE mice resulted from a reduction in D-serine release, we assessed the effect of a chronic administration of D-serine on the dendritic maturation of adult-born neurons in dnSNARE mice. Mice were injected with a RFP-expressing virus and withdrawn from Dox. Twenty-two days later, D-serine was injected daily for 8 days (50mg/kg, i.p from 22 to 29 dpi) and neuronal maturation was

examined at 30 dpi (Figure 7A). Consistent with blood-brain barrier permeability to D-serine (Pernot et al., 2012), intraperitoneal D-serine injections cancelled the difference in extracellular brain concentration between dnSNARE and WT mice (Figure 7B). In dnSNARE mice, D-serine administration restored dendritic length and arborization complexity of adult-born neurons to WT levels (Figure 7C-D) as well as the density and the size of dendritic protrusions (Figure 7E-G). D-serine also increased dendritic protrusion density on new neurons in WT mice (Figure 7E), but consistently with the observation that NMDAr co-agonists sites were depleted in dnSNARE mice, the effect of D-serine on spine density was greater in dnSNARE mice (56% increase) than in WT mice (33% increase). Similarly, the effect of D-serine on protrusion density was greater in dendritic segments crossing the territories of transgene-expressing astrocytes (inside; 110% increase) than outside (41%, Figure 7H-J).

The percentage of GFP$^+$ astrocytes and the density of GFAP$^+$ cells were similar between treated and untreated mice (Figure S7), indicating that D-serine did not modify the number of astrocytes expressing the transgene, or the total number of astrocytes.

Thus, the exogenous administration of D-serine restored defective dendritic maturation and formation of dendritic protrusions on newborn neurons in dnSNARE mice. Taken together, these results suggest an important role of astrocytic D-serine release in locally controlling synaptic integration of newly generated granule cells into the adult hippocampal circuitry.

DISCUSSION

This study provides direct *in vivo* evidence that astrocytes regulate the synaptic integration of new neurons in the adult hippocampus. By blocking exocytosis from a subset of astrocytes after the labeling and birth-dating of a cohort of newborn cells, we examined the role of astrocytes in the maturation of new hippocampal neurons. As schematized in supplemental Figure 8, we found that within their territories, individual astrocytes regulate synapse formation on adult-born neurons in a D-serine-dependent manner. This effect is crucial for the dendritic maturation and functional integration of new neurons, as well as for the survival of these cells during the critical period of their maturation. These results show that the maturation and synaptogenesis on adult-born neurons depends on cues provided by their direct cellular environment, namely astrocytes. These results have broad implications for the role of astrocytes in the adult brain and demonstrate that a molecule known to play a role in adult brain plasticity can also regulate the development of neurons generated in the adult brain.

Vesicular release from astrocytes and its role in neuronal function is a highly-debated topic, principally as a result from the intricate communication and interdependence between these two cell types. Recently, a study from Fujita et al. (Fujita et al., 2014), echoed by an expert opinion review (Sloan and Barres, 2014), has cast doubt on the role of astrocytic vesicular release in neuronal function. Indeed, Fujita et al. suggested that in one of the best transgenic mouse model to study astrocytic vesicular release so far, the dnSNARE mouse which we also examined in our study, neurons may also express small quantities of the transgenes and implied that results obtained with this mouse line may account for neuron-specific (rather than astrocyte-specific) effects. However, this study and the functional relevance of these measurements have been criticized (http://www.ncbi.nlm.nih.gov/pubmed/25505312/#comments). Furthermore, the results we present here do not support these conclusions for 2 reasons: First, the impairment in dendritic spine formation we observed here was only visible on new neurons and not on mature neurons, only upon withdrawal of Dox and, most importantly, were exclusively found on the dendritic portions that crossed the territories of transgene-expressing astrocytes. The reduction in dendritic spine density and maturation on the dendrites of newborn neurons followed exactly the borders of transgene-expressing astrocytes and returned to normal (i.e. similar to neurons newly-generated in wild-type mice) as soon as the same dendrites exited the territories of blocked astrocytes (Figure 2E). Second, these observations have been confirmed using iBot mice, expressing a different transgene inhibiting synaptobrevin-2 function (botulinum toxin instead of dnSNARE) using a different promoter (GLAST instead of GFAP) and a different induction system (tamoxifen-induced Cre recombinase instead of Dox) than the dnSNARE mouse. Together, these results indicate that the impaired development of new neurons cannot be explained by a –yet to be confirmed- neuronal expression of dnSNARE. Furthermore, they underline the necessity of fine morphological inspection to discriminate between astrocytic and neuronal protein localization. They also demonstrate that a careful morphological analysis, combined with the use of several controls, including internal controls, can unambiguously reveal astrocyte-specific effects on neurons.

D-serine is a co-agonist of the NMDA receptor (Schell et al., 1995) that regulates synaptic plasticity in the mature brain. By activating the glycine site of the NMDA receptor, D-serine enhances LTP induction (Bashir et al., 1990), whereas impaired exocytosis of D-serine from astrocytes reduces LTP expression in the hippocampus (Henneberger et al., 2010; Panatier et

al., 2006). Glutamate release from astrocytes has been shown to play a role in neuroblast migration from the subventricular zone to the olfactory bulb (Platel et al., 2010), but a role of D-serine in the synaptic integration of adult-born neurons was never reported. During their maturation, new granule neurons first receive GABAergic innervation (Li et al., 2012; Tozuka et al., 2005) which is excitatory, due to high intracellular chloride concentration (Chancey et al., 2013; Ge et al., 2008). Then, the first glutamatergic synaptic inputs on these cells express NMDA receptors and lack AMPA receptors thus forming silent synapses (Chancey et al., 2013; Schmidt-Salzmann et al., 2014). At this stage, GABA-mediated depolarization relieves the voltage-dependent Mg^{++} block from the NMDA receptors and enables their activation by glutamate. Such concomitant action of GABAergic and glutamatergic inputs enables the expression of AMPA receptors at the postsynaptic membrane and the unsilencing of newborn neurons (Chancey et al., 2013). In this context, the release of the NMDAr co-agonist D-serine by astrocytes represents an ideal way to promote this process and to contribute to the activity-dependent synaptic integration of new neurons. Consistent with this possibility, we observed that blocking astrocytic vesicular release resulted in impaired AMPAr currents, reduced maturation of dendritic spines and decreased survival of new neurons. These observations are in line with previous observations on the role of the NR1 subunit of the NMDA receptor on new neuron survival (Tashiro et al., 2007; Tashiro et al., 2006). They extent on these previous observations in showing that the impairment in survival is not detectable before glutamatergic synapse formation (at about 14 dpi) and extend until the end of synaptogenesis (between 30 and 90 dpi), suggesting that the formation excitatory synaptic inputs is crucial for the long-term survival of adult-born neurons. Our observations of reduced dendritic length and branching of new neurons in dnSNARE and iBot-Glast-CreER[T2] mice and also support previous reports of a role for NMDAr in dendritic development. Indeed, recent studies showed that the ablation of the NR2B subunit from newborn neurons reduces their dendritic complexity (Kheirbek et al., 2012) whereas learning experience enhances the dendritic maturation of new neurons in a NMDAr-dependent manner (Tronel et al., 2010).

Although our results clearly show an important role of D-serine in neuronal maturation in the adult brain, they do however not exclude the involvement of additional astrocyte-secreted molecules. Several other molecules are known to be released by astrocytes and to regulate synaptogenesis during development (Allen, 2013), such as Thrombospondin, Glypicans, TGFβ, TNFα, GABA or adenosine. In particular, adenosine is released in a synaptobrevin-2-dependent manner and its extracellular concentration may be reduced in dnSNARE mice (Schmitt et al., 2012). In the somato-sensory cortex, it was reported that a reduction of

extracellular adenosine concentration in dnSNARE mice decrease the amplitude of NMDA EPSCs and surface expression of NR2B subunits without affecting synaptic AMPA receptors (Deng et al., 2011). By contrast, in the adult hippocampus, we have observed a strong reduction of synaptic AMPA EPSCs, leading to an increase in the NMDA/AMPA ratio (Figure 4D). Furthermore, bath application of D-serine in slices largely rescued the NMDAr-deficit in newborn neurons in dnSNARE mice. Taken together, although we cannot exclude a further contribution of additional astrocyte-released factors, D-serine appears to make a major contribution to the local control of spine formation on newborn hippocampal granule neurons Dendritic protrusions express a constant number of NMDAr and a number of AMPAr that is correlated with the diameter of their tip (Takumi et al., 1999). Therefore, the structural correlate of silent synapses are dendritic protrusions with little or no enlargement of their tip, such as filopodia. Filopodia point towards and touch pre-existing axon terminals that are already involved in synapses with dendritic spines of other neurons. Upon conversion into dendritic spines, they form multiple synapse boutons, on which they compete with more mature neurons for stability on the axon terminal (Toni et al., 2007). In a recent study, we found that pre-existing, mature astrocytes ensheathe synapses on adult-born neurons independently of their age or the size of the dendritic protrusions (Krzisch et al., 2014). Thus, by contacting growing filopodia or immature dendritic spines, astrocytes are ideally positioned to supply D-serine to immature, silent dendritic protrusions, thereby enabling their maturation.

Astrocytes occupy distinct, non-overlapping territories (Bushong et al., 2002). The observation that individual astrocytes regulate the maturation of dendritic segments that intersect with their territories provides a clear demonstration that the structural boundaries of astrocytes delineate their functional impact on neurons. Since astrocytic vesicular release is regulated by neuronal activity (Bezzi and Volterra, 2001), individual astrocytes may serve as intermediates, coupling neuronal network activity to the local synaptic recruitment of adult-born neurons into the hippocampal synaptic circuitry. In turn, new neurons enhance the plasticity of neuronal networks into which they integrate (Schmidt-Hieber et al., 2004). Such "on demand" integration may serve to recruit new neurons in particularly active computational hotspots, thereby contributing to memory and the discrimination of learned events (Aimone and Gage, 2011). Conversely, astrocytic deficiency may result in impaired adult neurogenesis and cognitive deficits, as illustrated in Alexander's disease, which is

characterized by a mutated form of GFAP in astrocytes and results in impaired adult neurogenesis and learning performance (Hagemann et al., 2013).

Astrocytes are key constituents of the neurogenic niche and play a fundamental role in the regulation of neural progenitor proliferation (Song et al., 2002). We show here that, by providing the necessary cues, mature astrocytes enable the dendritic maturation, synaptic integration and survival of new neurons in the adult hippocampus. This regulation demonstrates a crucial role of the neurogenic niche in locally regulating and adjusting the late stages of adult neurogenesis, to fine tune network plasticity and hippocampal function.

Methods

Experimental animals:

dnSNARE mice were generated by crossing **1)** the GFAP-tTA line expressing the tet-off tetracycline transactivator under the control of the GFAP promoter and **2)** the tetO.dnSNARE line containing a tet-operator-regulated dominant-negative soluble N-ethylmaleimide-sensitive factor attachment protein receptor (dnSNARE) domain of synaptobrevin 2 as well as the reporter genes lacZ and GFP (Pascual et al., 2005).

iBot-Glast-CreER^{T2} mice were obtained by crossing 2 lines of transgenic mice (Slezak et al., 2012) : **1**) the iBot line, that contains a CAG (cytomegalovirus early enhancer and chicken beta-actin) promoter, a floxed-STOP cassette upstream of the gene encoding the *Clostridium botulinum* neurotoxin serotype B light chain (BoNT/B) followed by an GFP and **2**) the Glast-CreER^{T2} T45-72 line in which the expression of tamoxifen-inducible Cre recombinase (CreER^{T2}) is under the control of the astrocyte-specific promoter GLAST.

Stereotaxic viral injections:

Dividing neuronal progenitor cells and their progenies we identified and stably labeled using a MoMuLv encoding RFP or GFP under the control of the CAG promoter (Zhao et al., 2006). Viral injection was performed as previously described (Sultan et al., 2013). 1.5 ul of retroviral vector (final titer 10E8 pfu/ml) was injected in the DG (Bregma: -2 mm anteroposterior, 1,75

mm lateral and -2,00 mm dorsoventral) using a calibrated 5µl Hamilton syringe fitted with a 33-gauge needle.

Statistical analysis:

Hypothesis testing was two-tailed. All analyses were performed using JMP 10©. First, Shapiro-Wilk tests were performed on each group of data to test for distribution normality. When the distribution was not normal, a non-parametric Kruskal-Wallis test was used. Otherwise, analysis was performed using parametric tests. Homoscedasticity of variances was tested by Bartlett's or Levene's tests and adequate analysis of variance (ANOVA or Welch's ANOVA) was performed, followed by a post-hoc multiple comparisons procedure Tukey's HSD test or t-test with Bonferonni correction. For two sample comparisons, when the distribution was normal, the equality of variance of the groups was tested by a bilateral F-test and the adequate unpaired t-test was used. When the distribution was not normal, a Mann-Whitney test was used. For the Sholl analysis, parametric tests were used: Two-Way ANOVA with repeated measures was performed, followed by a post-hoc Tukey's HSD test. All data are presented as mean ± s.e.m.

AUTHOR CONTRIBUTIONS:

N.T., J.B., P.B. and S.S., conceived and designed the experiments. S.S., L.L., J.M., F.Pe., E.G., J.L. and P.B. performed the experiments. S.S., L.L., J.M., F.C., P.B., J.B, and N.T analyzed and discussed the data. S.S., F.Pf., J.B. and N.T. wrote the manuscript. N.T., F.Pf., J.B and P.B. provided financial support.

ACKNOWLEDGMENTS:

(J.M), the NCCR "Transcure" and NCCR "Synapsy" (P.B., F.Pe.), ANR GLIAVAMP and ASTREX and DFG (F.Pf.).

FIGURE LEGENDS:

Figure 1: BoNT expression in astrocytes impairs the maturation and survival of new neurons as well as dendritic spine formation

(**A**) Confocal micrographs of the dentate gyrus of iBot-Glast-CreER^{T2} mice, before and 3 weeks after the induction of transgene expression with tamoxifen (Tam) injections showing the mosaic pattern of transgene expression (Scale bar, left and middle panels 100µm, right panel 50µm). (**B**) Confocal micrograph of GFAP immunostaining (red) on a iBot-Glast-CreER^{T2} Tam injected mouse hippocampal section showing the mosaic pattern of transgene expression. Scale bar, 50 µm. (**C**) Experimental timeline: iBot-Glast-CreER^{T2} (n=5 mice) were injected with BrdU (3 injections IP, 100 mg/kg every 2 hours) followed one day later by an intrahippocampal injection with a RFP-encoding moloney virus (day 0). Transgene expression was induced by daily injections of Tam from 7 to 11 days post virus injection (dpi) and hippocampal slices were analyzed at 30 dpi. Control animals consisted of tamoxifen-injected animals (Ctrl+Tam: n=3 monogenic iBot + 2 WT littermate mice) and animals injected with vehicle (Ctrl No Tam: n=2 iBot-Glast-CreER^{T2} + 1 WT mice). (**D**) Confocal micrographs of spiny dendrites from new neurons in iBot-Glast-CreER^{T2} injected with Tam intersecting with (inside) and exiting (outside) transgene-expressing astrocytes. Scale bar, 5µm. (**E**) Dendritic protrusion density on adult-born neurons in dendritic segments inside and outside of transgene-expressing astrocytes (bilateral Student's t-test, ***P<0.001). (**F**) Proportion of protrusions with filopodia (F), thin (T) and mushroom (M, See methods section) morphologies. The proportion of filopodia was greater (bilateral Student's t-test, ***P<0.001) and the proportion of mushroom spines was smaller (Mann-Whitney test, *P<0.05) in dendritic segments intersecting transgene-expressing astrocytes in iBot-Glast-CreER^{T2} injected with Tam. (**G**) Confocal micrographs of dendrites of newborn neurons from iBot-Glast-CreER^{T2} injected with tamoxifen (iBot-Glast + Tam) and control mice. Scale bar, 5µm. (**H**) The global dendritic protrusion density on new neurons was smaller in iBot-Glast + Tam than control mice (One-Way ANOVA, $F_{2,12}$=22,2036, P=0,0002; post-hoc Tukey's HSD test, *P<0.05). (**I**) The proportion of mushroom spines on adult-born neurons was smaller in iBot-Glast + Tam than in control mice (Filopodia (F) One-Way ANOVA $F_{2,12}$ =1.9260, P=0.1961, Thin (T) One-Way ANOVA $F_{2,12}$=0.042, P=0.9590 and Mushroom (M), One-Way ANOVA

$F_{2,12}=7.47$, P=0.0103; post-hoc Tukey's HSD test, *P<0.05). (**J**) Confocal micrographs (left panels) and 3D reconstructions (right panels) of RFP$^+$ new neurons at 30 dpi. Scale bar, 20µm. (**K**) Newborn neurons dendritic length (One-Way ANOVA; post-hoc Tukey's HSD test, *P<0.05; **P<0.01). (**L**) Scholl analysis of dendritic complexity (Two-Way ANOVA with repeated measures $F_{2,10}=1.18$, P=0.34). (**M**) Number of new neurons (co-expressing BrdU and Neu-N) in the DG (One-Way ANOVA $F_{2,12}=12.55$, P=0.0019; post-hoc Tukey's HSD test, **P<0.01). Values represent the mean ± s.e.m.

Figure 2: dnSNARE expression in astrocytes impairs the maturation and survival of new neurons as well as dendritic spine formation

(**A**) Experimental timeline: Dox was withdrawn immediately after virus injection and mice were analyzed 30 days later. (**B-C**) Confocal micrographs of dendritic segments of new neurons (red) extending inside and outside of transgene-expressing astrocytes (green). (**D**) Confocal micrographs of dendrites of new neurons in dnSNARE mice. Right panel shows dendrites that extend into transgene-expressing astrocytes (inside) as well as into astrocytes not expressing the transgenes (outside). Note the thinner dendritic diameter and lower spine density of the dendrites upon entering transgene-expressing astrocyte territories. (**E**) Line plot of the dendritic protrusion density along several dendritic segments for a total cumulated length of 1000 µm. Individual dendritic segments are separated by a blank space. Note the heterogeneity in spine density along dendrites in dnSNARE mice. (**F-G**) Summaries of protrusions density (F, Bilateral Student's t-test) and proportion of protrusions with filopodia (F), thin (T) and mushroom (M) morphologies in the different segments (G, Bilateral Student's t-test for F and M and Welch's t-test for T, *P<0.05). (**H**) Correlation between the proportion of dendritic length of new neurons that intersects transgene-expressing astrocytes and the decrease in protrusion density (Spearman's ρ=0.6304; P<0.0001). (**I-J**) Histogram of the global protrusion density (I, One-Way ANOVA: $F_{2,14}=19.22$, P<0.0001 followed by post-hoc Tukey's HSD) and morphology (J, One-Way ANOVA followed by post-hoc Tukey's HSD: Filopodia (F) $F_{2,14}=14.67$, p=0.0006; Thin (T) $F_{2,14}=11.64$, p=0.0015 and Mushroom (M) $F_{2,14}=3.71$, p=0.0555) of newborn neurons in WT, single transgenic and dnSNARE mice. (**K**) 3D reconstructions of new neurons from WT and dnSNARE mice. Scale bar 50µm. (**L**) Scholl analysis of dendritic branching (Two-Way ANOVA $F_{2,12}=12.25$, P=0.0013 followed by post-hoc Tukey's HSD). (**M**) Dendritic length of new neurons (One-Way ANOVA $F_{2,14}=6.5917$, P=0,0117 followed by post-hoc Tukey's HSD). (**N**) Correlation between dendritic length and coverage by transgene-expressing astrocytes (Spearman's ρ= -0.4734;

P=0.0005). (**O**) Experimental timeline: Dox was withdrawn immediately after BrdU injections and mice were analyzed 1 or 30 days later. (**P**) Confocal micrographs of BrdU-NeuN labeling of new neurons at 30 dpi, scale bars: 10 μm. (**Q**) Number of BrdU$^+$ cells at 1dpi (One-Way ANOVA $F_{2,12}$=0.04, P=0,9517). (**R**) Number BrdU$^+$-NeuN$^+$ surviving neurons at 30 dpi (One-Way ANOVA $F_{2,12}$=31.10, P<0.0001 followed by post-hoc Tukey's HSD). For all, values represent the means ± s.e.m. NS P>0.05, *P<0.05, **P<0.01, ***P<0.0001.

Figure 3: The fine structure of perisynaptic processes of dnSNARE-expressing astrocytes is similar to WT

(**A**) Peroxidase-labeled new neuron dendrite (30 dpi) intersecting the territory of an immunoperoxidase-labeled transgene-expressing astrocyte that was further examined with electron microscopy. (**B**) Electron micrographs of the same region, showing the labeled dendrite (red) and astrocyte (green). (**C**) This astrocyte and dendrite were serially sectioned and 3D reconstructed. Two axons (yellow) forming synaptic contacts (arrowheads) with adult-born neuron dendritic spines (red), inside and outside of the transgene-expressing astrocyte (green). Processes of an astrocyte not expressing the transgene (blue) has been reconstructed for comparison. Scale bars: **A** 20 μm, **B** 10 μm, **C** 5μm. (**D**) 3D reconstructions from electron micrographs of dendritic spines and their perisynaptic processes. In dnSNARE and WT mice, newborn neurons (GFP$^+$) are shown in red and random neurons (GFP$^-$) in purple. Also shown are some axon terminals (yellow) and all astrocytic perisynaptic processes (green in GFP$^+$ astrocytes, blue outside GFP$^+$ astrocytes and in WT mice). Scale bars: 0.5μm. (**E**) Histogram showing the proportion of synaptic surface area (from new neuron or from random neurons) that is ensheathed by dnSNARE-expressing astrocyte, astrocyte not expressing dnSNARE, or WT astrocyte (Kruskal–Wallis, P=0.6185). Each value represents the mean ± s.e.m.

Figure 4: Impaired NMDA- and AMPA- mediated synaptic transmission in newborn neurons in dnSNARE mice

(**A**) AMPAr- and NMDAr-mediated excitatory postsynaptic currents (EPSC, recorded at -80 mV and +40 mV respectively) in adult-born neurons from WT and dnSNARE mice at 30 dpi. Dotted line indicates 0 pA. (**B**) Histogram of the AMPAr-EPSCs in new neurons from dnSNARE and WT mice (WT: 340.5±42.0 pA, dnSNARE: 109.5±23.0 pA; p=0.0005, non-parametric Mann Whitney test; n=9 and 11, respectively). (**C**) Histogram of the NMDAr-EPSC currents in adult-born neurons from WT and dnSNARE mice at 30 dpi (WT: 201.3±24.9 pA, dnSNARE: 95.0±12.8 pA; p=0.005, nonparametric Mann Whitney test; n=9

and 11 for WT and dnSNARE, respectively). (**D**) NMDA EPSC/AMPA EPSC ratio in adult-born neurons from WT and dnSNARE mice at 30 dpi (WT: 1.21±0.10, dnSNARE: 2.35 ±0.37; p=0.01, nonparametric Mann Whitney test; n=9 and 11 for WT and dnSNARE, respectively). (**E-F**) Example traces of 6-second recordings of miniature EPSCs (mEPSCs) from newly-generated neurons in WT and dnSNARE mice, as indicated. (**G**) Cumulative probability plot of inter-event intervals (IEIs) of all mEPSCs recorded from newborn neurons in WT and dnSNARE mice, respectively. Longer average mEPSC interval was detected in dnSNARE mice (WT: 0.71±0.01 s, total 3460 events from 8 cells, dnSNARE: 1.10±0.03 s, total 1606 events from 6 cells. p<0.001, nonparametric Kolmogorov-Smirnov test). (**H**) Cumulative probability plot of mEPSCs amplitude from newborn neurons in WT and dnSNARE mice, respectively (WT: 8.37±0.13 pA, total 3468 events from 8 cells, dnSNARE: 6.87±0.15 pA, total 1612 events from 6 cells. p<0.001, nonparametric Kolmogorov-Smirnov test). (**I**) Typical average mEPSCs obtained from single newborn neurons in a WT or dnSNARE mouse. (**J**) Histogram of the mEPSC decay time constant in new neurons of WT and dnSNARE mice (WT: 8.48±0.79 ms, dnSNARE: 10.03±0.96 ms. p=0.23, nonparametric Mann Whitney test. n=6 and 8 for WT and dnSNARE mice, respectively). Each value represents the mean ± s.e.m.

Figure 5: Pre-established spines are not destabilized by dnSNARE expression in astrocytes

(**A**) Experimental timeline: Moloney virus was injected 30 days before Dox removal. Mice were sacrificed and examined at 30 or 60 days post injection (dpi). (**B**) Dendritic protrusion density at 30 and 60 dpi (One-Way ANOVA $F_{3,15}$=18.61, P<0,0001 followed by post-hoc Tukey's HSD) (**C**) Dendritic protrusion morphology on new neurons in dnSNARE or WT mice at 60 dpi. (**D**) Dendritic protrusion density at 60 dpi in dendritic segments inside or outside of transgene-expressing astrocytes. (**E**) Dendritic protrusion morphology at 60 dpi in dendritic segments inside or outside of transgene-expressing astrocytes. (**F**) Experimental timeline: Dox was removed and 30 days later, mice were sacrificed and random dendrites were labeled with the lipophilic die DiI. (**G**) Confocal micrographs of DiI-labeled dendrites (red). Scale bar: 5µm. (**H**) Dendritic protrusion density on entire DiI-labeled dendrites and (**I**) on dendritic segments inside or outside of transgene-expressing astrocytes. For all, each value represents the mean +/- s.e.m. Bilateral Student's t-test for all. NS: P>0.05, *P<0.05, **P<0.01.

Figure 6: In dnSNARE mice, extracellular D-serine is reduced and its exogenous application partially rescues NMDAr EPSCs in newborn neurons

(**A**) Experimental timeline: microdialysis was performed in the DG 30 days after Dox withdrawal. (**B**) Extracellular concentration of D-serine, Glycine, Glutamate and GABA in the DG of dnSNARE and WT mice analyzed by HPLC (n=5-6 mice per group, nonparametric Wilcoxon test for each molecule). (**C**) Sample confocal images of GFAP immunostained hippocampal astrocytic culture from WT and dnSNARE mice. In dnSNARE astrocytic culture 60% ($\pm$ 8.5%) of astrocytes expressed GFP. Scale bar, 20µm. (**D**) Concentration of proteins (mg/ml) measured in astrocytic culture used to condition the medium analyzed by HPLC (3 samples per group, nonparametric Wilcoxon test). (**E**) HPCL analysis of D-serine concentration in medium conditioned by dnSNARE and WT astrocytes (3 samples per group, nonparametric Wilcoxon test). (**F**) Example traces of NMDAr-EPSCs (recorded at +40 mV) prior to (in black) and during 50 µM D-serine application (in blue) in newborn neurons from WT and dnSNARE mice at 30dpi; (**G**) NMDAr-EPSC amplitude prior to and during D-serine application in newborn neurons from WT mice at 30dpi (211.1$\pm$25.9 pA and 184.8$\pm$14.0 pA. p=0.06, non-parametric Wilcoxon matched pairs test, n=8 pairs). (**H**) NMDAr-EPSC amplitude prior to and during D-serine application in newborn neurons from dnSNARE mice at 30dpi (88.4$\pm$14.8 pA and 134.1$\pm$24.2 pA. nonparametric Wilcoxon matched pairs test, n=9 pairs). The dashed red line (in **G** and **H**) indicates the mean NMDAr-EPSC amplitude in newborn neurons from WT mice, as shown in **Fig.4. C**. Values represent the mean $\pm$ s.e.m. NS: not significant, *P<0.05, **P<0.01.

Figure 7: D-serine administration restores the maturation of new neurons in dnSNARE mice.

(**A**) Experimental timeline: Dox was withdrawn immediately after viral injection and D-serine (50 mg/kg, ip) or vehicle (NaCl 0.9%) was injected daily, from 22 to 29 dpi. Mice were analyzed at 30 dpi. (**B**) Extracellular concentration of D-serine in the DG of dnSNARE and WT mice treated with D-serine (n=5-6 mice per group, nonparametric Wilcoxon test). (**C-D**) Histogram of the total dendritic length (**C**, One-Way ANOVA $F_{3,19}$=8.5882, p=0,0013 followed by post-hoc Tukey's HSD) and dendritic arborization complexity (**D**, Two-Way ANOVA with repeated measures $F_{3,16}$=18.55, p<0.0001 followed by post-hoc Tukey's HSD) of newborn in dnSNARE and WT mice after D-serine or vehicle injections. (**E-G**) Histogram

of the dendritic protrusion density (**E**, One-Way ANOVA $F_{2,17}$=23.33, P<0,0001 followed by post-hoc Tukey's HSD) and their morphology in newborn neurons of dnSNARE and WT mice after vehicle (**F**) or D-serine (**G**) treatment (bilateral Student's t-test between categories filopodia (F), thin (T) or mushroom (M)). (**H-J**) Histogram of the protrusion density (**H**, One-Way ANOVA $F_{3,19}$=60.60, P<0,0001 followed by post-hoc Tukey's HSD) and their morphology in newborn neurons of dnSNARE inside (in green) and outside (in red) transgene-expressing astrocytes after vehicle or D-serine (**J**) injections (bilateral Student's t-test between categories filopodia (F), thin (T) or mushroom (M)). For all, each value represents the mean +/- s.e.m. NS: not significant, *P<0.05, **P<0.01, ***P<0.001.

REFERENCES:

Aimone, J.B., and Gage, F.H. (2011). Modeling new neuron function: a history of using computational neuroscience to study adult neurogenesis. The European journal of neuroscience 33, 1160-1169.

Allen, N.J. (2013). Role of glia in developmental synapse formation. Current opinion in neurobiology 23, 1027-1033.

Allen, N.J., Bennett, M.L., Foo, L.C., Wang, G.X., Chakraborty, C., Smith, S.J., and Barres, B.A. (2012). Astrocyte glypicans 4 and 6 promote formation of excitatory synapses via GluA1 AMPA receptors. Nature 486, 410-414.

Altman, J., and Das, G.D. (1965). Autoradiographic and histological evidence of postnatal hippocampal neurogenesis in rats. J Comp Neurol 124, 319-335.

Araque, A., Carmignoto, G., Haydon, P.G., Oliet, S.H., Robitaille, R., and Volterra, A. (2014). Gliotransmitters travel in time and space. Neuron 81, 728-739.

Banker, G.A. (1980). Trophic interactions between astroglial cells and hippocampal neurons in culture. Science 209, 809-810.

Bashir, Z.I., Tam, B., and Collingridge, G.L. (1990). Activation of the glycine site in the NMDA receptor is necessary for the induction of LTP. Neuroscience letters 108, 261-266.

Bergami, M., and Berninger, B. (2012). A fight for survival: the challenges faced by a newborn neuron integrating in the adult hippocampus. Developmental neurobiology 72, 1016-1031.

Bezzi, P., and Volterra, A. (2001). A neuron-glia signalling network in the active brain. Current opinion in neurobiology 11, 387-394.

Bruel-Jungerman, E., Davis, S., Rampon, C., and Laroche, S. (2006). Long-term potentiation enhances neurogenesis in the adult dentate gyrus. The Journal of neuroscience : the official journal of the Society for Neuroscience 26, 5888-5893.

Bushong, E.A., Martone, M.E., and Ellisman, M.H. (2004). Maturation of astrocyte morphology and the establishment of astrocyte domains during postnatal hippocampal development. International journal of developmental neuroscience : the official journal of the International Society for Developmental Neuroscience 22, 73-86.

Bushong, E.A., Martone, M.E., Jones, Y.Z., and Ellisman, M.H. (2002). Protoplasmic astrocytes in CA1 stratum radiatum occupy separate anatomical domains. The Journal of neuroscience : the official journal of the Society for Neuroscience 22, 183-192.

Cao, X., Li, L.P., Qin, X.H., Li, S.J., Zhang, M., Wang, Q., Hu, H.H., Fang, Y.Y., Gao, Y.B., Li, X.W., *et al.* (2013). Astrocytic adenosine 5'-triphosphate release regulates the proliferation of neural stem cells in the adult hippocampus. Stem cells 31, 1633-1643.

Chancey, J.H., Adlaf, E.W., Sapp, M.C., Pugh, P.C., Wadiche, J.I., and Overstreet-Wadiche, L.S. (2013). GABA depolarization is required for experience-dependent synapse unsilencing in adult-born neurons. The Journal of neuroscience : the official journal of the Society for Neuroscience 33, 6614-6622.

Chancey, J.H., Poulsen, D.J., Wadiche, J.I., and Overstreet-Wadiche, L. (2014). Hilar mossy cells provide the first glutamatergic synapses to adult-born dentate granule cells. The Journal of neuroscience : the official journal of the Society for Neuroscience 34, 2349-2354.

Christopherson, K.S., Ullian, E.M., Stokes, C.C., Mullowney, C.E., Hell, J.W., Agah, A., Lawler, J., Mosher, D.F., Bornstein, P., and Barres, B.A. (2005). Thrombospondins are astrocyte-secreted proteins that promote CNS synaptogenesis. Cell 120, 421-433.

Deng, Q., Terunuma, M., Fellin, T., Moss, S.J., and Haydon, P.G. (2011). Astrocytic activation of A1 receptors regulates the surface expression of NMDA receptors through a Src kinase dependent pathway. Glia 59, 1084-1093.

Eriksson, P.S., Perfilieva, E., Bjork-Eriksson, T., Alborn, A.M., Nordborg, C., Peterson, D.A., and Gage, F.H. (1998). Neurogenesis in the adult human hippocampus. Nat Med 4, 1313-1317.

Fellin, T., Halassa, M.M., Terunuma, M., Succol, F., Takano, H., Frank, M., Moss, S.J., and Haydon, P.G. (2009). Endogenous nonneuronal modulators of synaptic transmission control cortical slow oscillations in vivo. Proc Natl Acad Sci U S A 106, 15037-15042.

Fujita, T., Chen, M.J., Li, B., Smith, N.A., Peng, W., Sun, W., Toner, M.J., Kress, B.T., Wang, L., Benraiss, A., *et al.* (2014). Neuronal transgene expression in dominant-negative SNARE mice. The Journal of neuroscience : the official journal of the Society for Neuroscience 34, 16594-16604.

Ge, S., Goh, E.L., Sailor, K.A., Kitabatake, Y., Ming, G.L., and Song, H. (2006). GABA regulates synaptic integration of newly generated neurons in the adult brain. Nature 439, 589-593.

Ge, S., Sailor, K.A., Ming, G.L., and Song, H. (2008). Synaptic integration and plasticity of new neurons in the adult hippocampus. J Physiol 586, 3759-3765.

Ge, S., Yang, C.H., Hsu, K.S., Ming, G.L., and Song, H. (2007). A critical period for enhanced synaptic plasticity in newly generated neurons of the adult brain. Neuron 54, 559-566.

Ge, W.P., Miyawaki, A., Gage, F.H., Jan, Y.N., and Jan, L.Y. (2012). Local generation of glia is a major astrocyte source in postnatal cortex. Nature 484, 376-380.

Hagemann, T.L., Paylor, R., and Messing, A. (2013). Deficits in adult neurogenesis, contextual fear conditioning, and spatial learning in a Gfap mutant mouse model of Alexander disease. The Journal of neuroscience : the official journal of the Society for Neuroscience 33, 18698-18706.

Henneberger, C., Papouin, T., Oliet, S.H., and Rusakov, D.A. (2010). Long-term potentiation depends on release of D-serine from astrocytes. Nature 463, 232-236.

Kartvelishvily, E., Shleper, M., Balan, L., Dumin, E., and Wolosker, H. (2006). Neuron-derived D-serine release provides a novel means to activate N-methyl-D-aspartate receptors. J Biol Chem 281, 14151-14162.

Kempermann, G., and Gage, F.H. (1999). Experience-dependent regulation of adult hippocampal neurogenesis: effects of long-term stimulation and stimulus withdrawal. Hippocampus 9, 321-332.

Kheirbek, M.A., Tannenholz, L., and Hen, R. (2012). NR2B-dependent plasticity of adult-born granule cells is necessary for context discrimination. The Journal of neuroscience : the official journal of the Society for Neuroscience 32, 8696-8702.

Kronenberg, G., Reuter, K., Steiner, B., Brandt, M.D., Jessberger, S., Yamaguchi, M., and Kempermann, G. (2003). Subpopulations of proliferating cells of the adult hippocampus respond differently to physiologic neurogenic stimuli. J Comp Neurol 467, 455-463.

Krzisch, M., Temprana, S.G., Mongiat, L.A., Armida, J., Schmutz, V., Virtanen, M.A., Kocher-Braissant, J., Kraftsik, R., Vutskits, L., Conzelmann, K.K., *et al.* (2014). Pre-existing astrocytes form functional perisynaptic processes on neurons generated in the adult hippocampus. Brain Struct Funct.

Li, Y., Aimone, J.B., Xu, X., Callaway, E.M., and Gage, F.H. (2012). Development of GABAergic inputs controls the contribution of maturing neurons to the adult hippocampal network. Proc Natl Acad Sci U S A 109, 4290-4295.

Martineau, M., Shi, T., Puyal, J., Knolhoff, A.M., Dulong, J., Gasnier, B., Klingauf, J., Sweedler, J.V., Jahn, R., and Mothet, J.P. (2013). Storage and uptake of D-serine into astrocytic synaptic-like vesicles specify gliotransmission. The Journal of neuroscience : the official journal of the Society for Neuroscience 33, 3413-3423.

Matsuzaki, M., Ellis-Davies, G.C., Nemoto, T., Miyashita, Y., Iino, M., and Kasai, H. (2001). Dendritic spine geometry is critical for AMPA receptor expression in hippocampal CA1 pyramidal neurons. Nature neuroscience 4, 1086-1092.

Mauch, D.H., Nagler, K., Schumacher, S., Goritz, C., Muller, E.C., Otto, A., and Pfrieger, F.W. (2001). CNS synaptogenesis promoted by glia-derived cholesterol. Science 294, 1354-1357.

Nishida, H., and Okabe, S. (2007). Direct astrocytic contacts regulate local maturation of dendritic spines. The Journal of neuroscience : the official journal of the Society for Neuroscience 27, 331-340.

Okamoto, M., Inoue, K., Iwamura, H., Terashima, K., Soya, H., Asashima, M., and Kuwabara, T. (2011). Reduction in paracrine Wnt3 factors during aging causes impaired adult neurogenesis. FASEB journal : official publication of the Federation of American Societies for Experimental Biology 25, 3570-3582.

Panatier, A., Theodosis, D.T., Mothet, J.P., Touquet, B., Pollegioni, L., Poulain, D.A., and Oliet, S.H. (2006). Glia-derived D-serine controls NMDA receptor activity and synaptic memory. Cell 125, 775-784.

Pascual, O., Casper, K.B., Kubera, C., Zhang, J., Revilla-Sanchez, R., Sul, J.Y., Takano, H., Moss, S.J., McCarthy, K., and Haydon, P.G. (2005). Astrocytic purinergic signaling coordinates synaptic networks. Science 310, 113-116.

Pernot, P., Maucler, C., Tholance, Y., Vasylieva, N., Debilly, G., Pollegioni, L., Cespuglio, R., and Marinesco, S. (2012). d-Serine diffusion through the blood-brain barrier: effect on d-serine compartmentalization and storage. Neurochem Int 60, 837-845.

Pfrieger, F.W., and Barres, B.A. (1997). Synaptic efficacy enhanced by glial cells in vitro. Science 277, 1684-1687.

Platel, J.C., Dave, K.A., Gordon, V., Lacar, B., Rubio, M.E., and Bordey, A. (2010). NMDA receptors activated by subventricular zone astrocytic glutamate are critical for neuroblast survival prior to entering a synaptic network. Neuron 65, 859-872.

Schell, M.J., Molliver, M.E., and Snyder, S.H. (1995). D-serine, an endogenous synaptic modulator: localization to astrocytes and glutamate-stimulated release. Proc Natl Acad Sci U S A 92, 3948-3952.

Schiavo, G., Benfenati, F., Poulain, B., Rossetto, O., Polverino de Laureto, P., DasGupta, B.R., and Montecucco, C. (1992). Tetanus and botulinum-B neurotoxins block neurotransmitter release by proteolytic cleavage of synaptobrevin. Nature 359, 832-835.

Schmidt-Hieber, C., Jonas, P., and Bischofberger, J. (2004). Enhanced synaptic plasticity in newly generated granule cells of the adult hippocampus. Nature 429, 184-187.

Schmidt-Salzmann, C., Li, L., and Bischofberger, J. (2014). Functional properties of extrasynaptic AMPA and NMDA receptors during postnatal hippocampal neurogenesis. J Physiol 592, 125-140.

Schmitt, L.I., Sims, R.E., Dale, N., and Haydon, P.G. (2012). Wakefulness affects synaptic and network activity by increasing extracellular astrocyte-derived adenosine. The Journal of neuroscience : the official journal of the Society for Neuroscience 32, 4417-4425.

Slezak, M., Grosche, A., Niemiec, A., Tanimoto, N., Pannicke, T., Munch, T.A., Crocker, B., Isope, P., Hartig, W., Beck, S.C., *et al.* (2012). Relevance of exocytotic glutamate release from retinal glia. Neuron 74, 504-516.

Sloan, S.A., and Barres, B.A. (2014). Looks can be deceiving: reconsidering the evidence for gliotransmission. Neuron 84, 1112-1115.

Song, H., Stevens, C.F., and Gage, F.H. (2002). Astroglia induce neurogenesis from adult neural stem cells. Nature 417, 39-44.

Sultan, S., Gebara, E., and Toni, N. (2013). Doxycycline increases neurogenesis and reduces microglia in the adult hippocampus. Front Neurosci 7, 131.

Sun, W., McConnell, E., Pare, J.F., Xu, Q., Chen, M., Peng, W., Lovatt, D., Han, X., Smith, Y., and Nedergaard, M. (2013). Glutamate-dependent neuroglial calcium signaling differs between young and adult brain. Science 339, 197-200.

Takumi, Y., Ramirez-Leon, V., Laake, P., Rinvik, E., and Ottersen, O.P. (1999). Different modes of expression of AMPA and NMDA receptors in hippocampal synapses. Nature neuroscience 2, 618-624.

Tashiro, A., Makino, H., and Gage, F.H. (2007). Experience-specific functional modification of the dentate gyrus through adult neurogenesis: a critical period during an immature stage. The Journal of neuroscience : the official journal of the Society for Neuroscience 27, 3252-3259.

Tashiro, A., Sandler, V.M., Toni, N., Zhao, C., and Gage, F.H. (2006). NMDA-receptor-mediated, cell-specific integration of new neurons in adult dentate gyrus. Nature 442, 929-933.

Toni, N., and Sultan, S. (2011). Synapse formation on adult-born hippocampal neurons. The European journal of neuroscience 33, 1062-1068.

Toni, N., Teng, E.M., Bushong, E.A., Aimone, J.B., Zhao, C., Consiglio, A., van Praag, H., Martone, M.E., Ellisman, M.H., and Gage, F.H. (2007). Synapse formation on neurons born in the adult hippocampus. Nature neuroscience 10, 727-734.

Tozuka, Y., Fukuda, S., Namba, T., Seki, T., and Hisatsune, T. (2005). GABAergic excitation promotes neuronal differentiation in adult hippocampal progenitor cells. Neuron 47, 803-815.
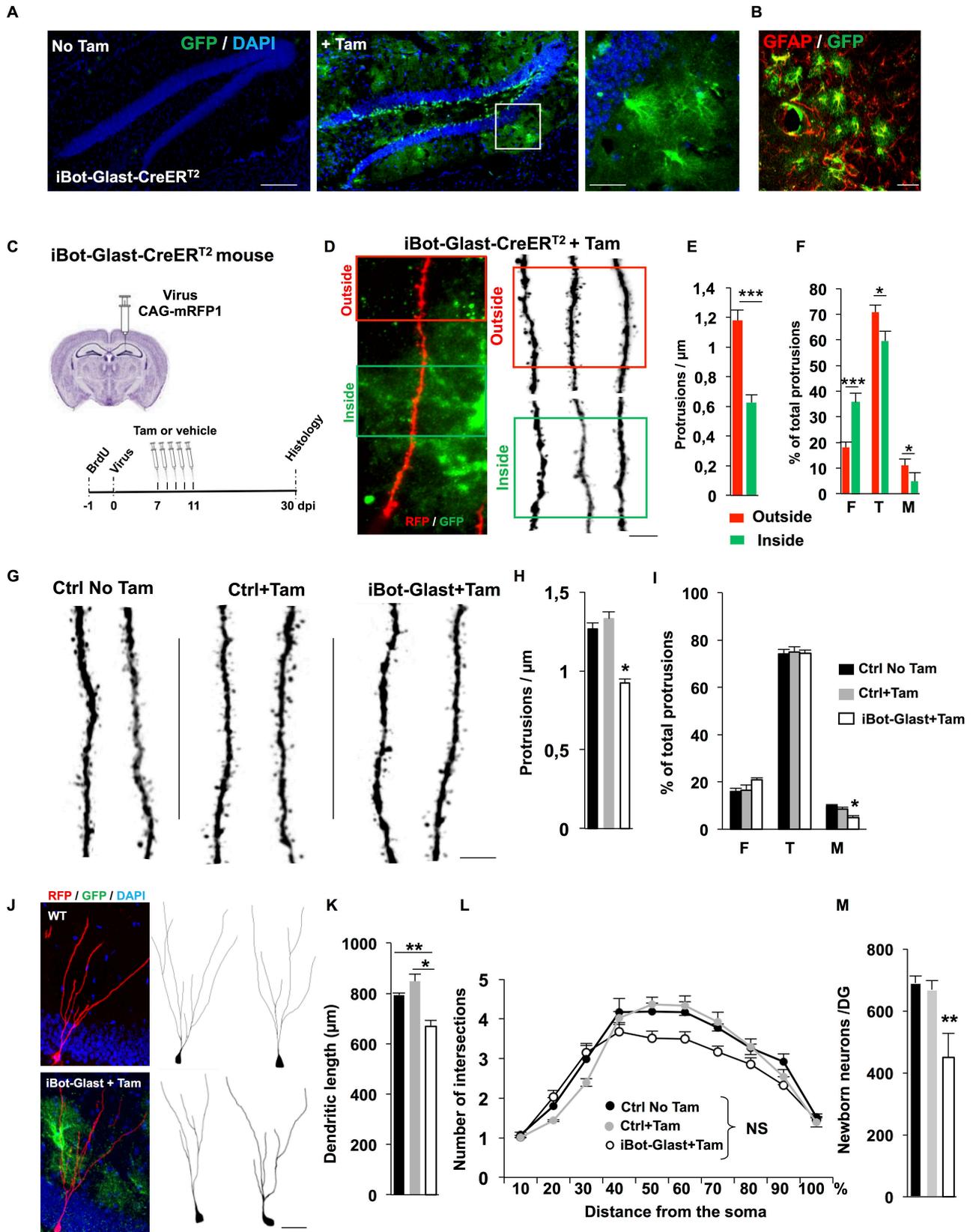
Tronel, S., Fabre, A., Charrier, V., Oliet, S.H., Gage, F.H., and Abrous, D.N. (2010). Spatial learning sculpts the dendritic arbor of adult-born hippocampal neurons. Proc Natl Acad Sci U S A 107, 7963-7968.

Zhao, C., Deng, W., and Gage, F.H. (2008). Mechanisms and functional implications of adult neurogenesis. Cell 132, 645-660.

Zhao, C., Teng, E.M., Summers, R.G., Jr., Ming, G.L., and Gage, F.H. (2006). Distinct morphological stages of dentate granule neuron maturation in the adult mouse

hippocampus. The Journal of neuroscience : the official journal of the Society for Neuroscience 26, 3-11.
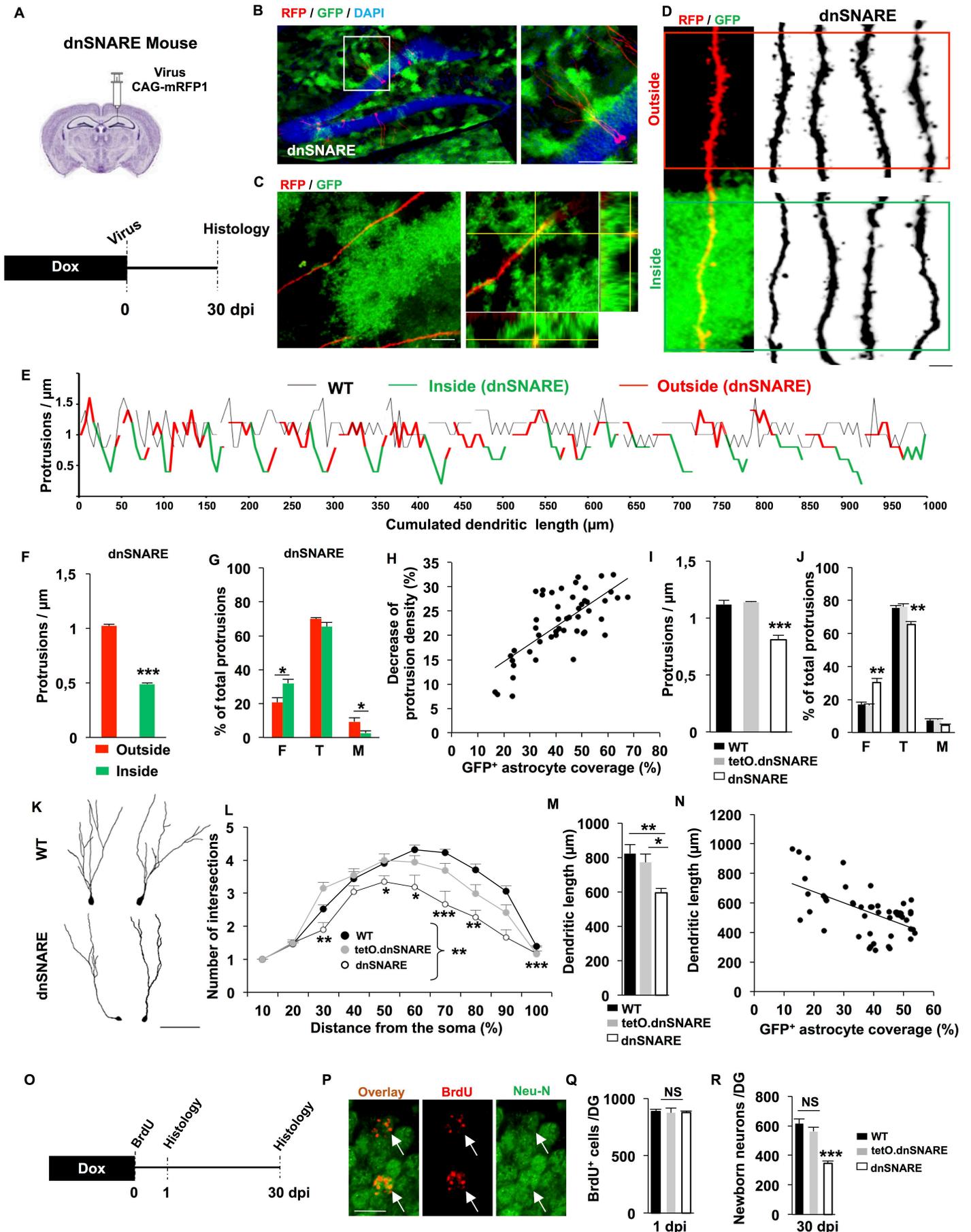
Figure 1

Figure 2

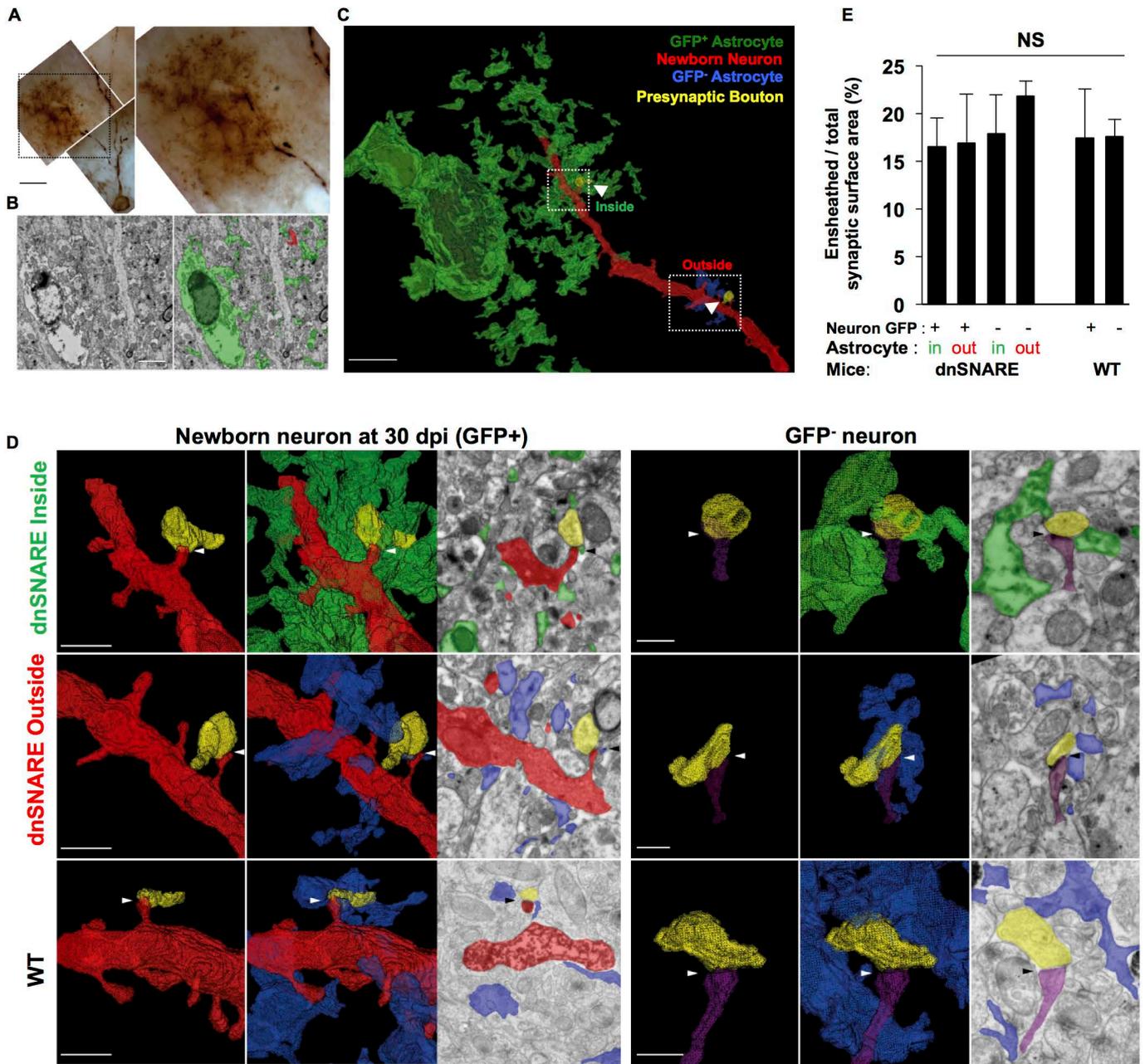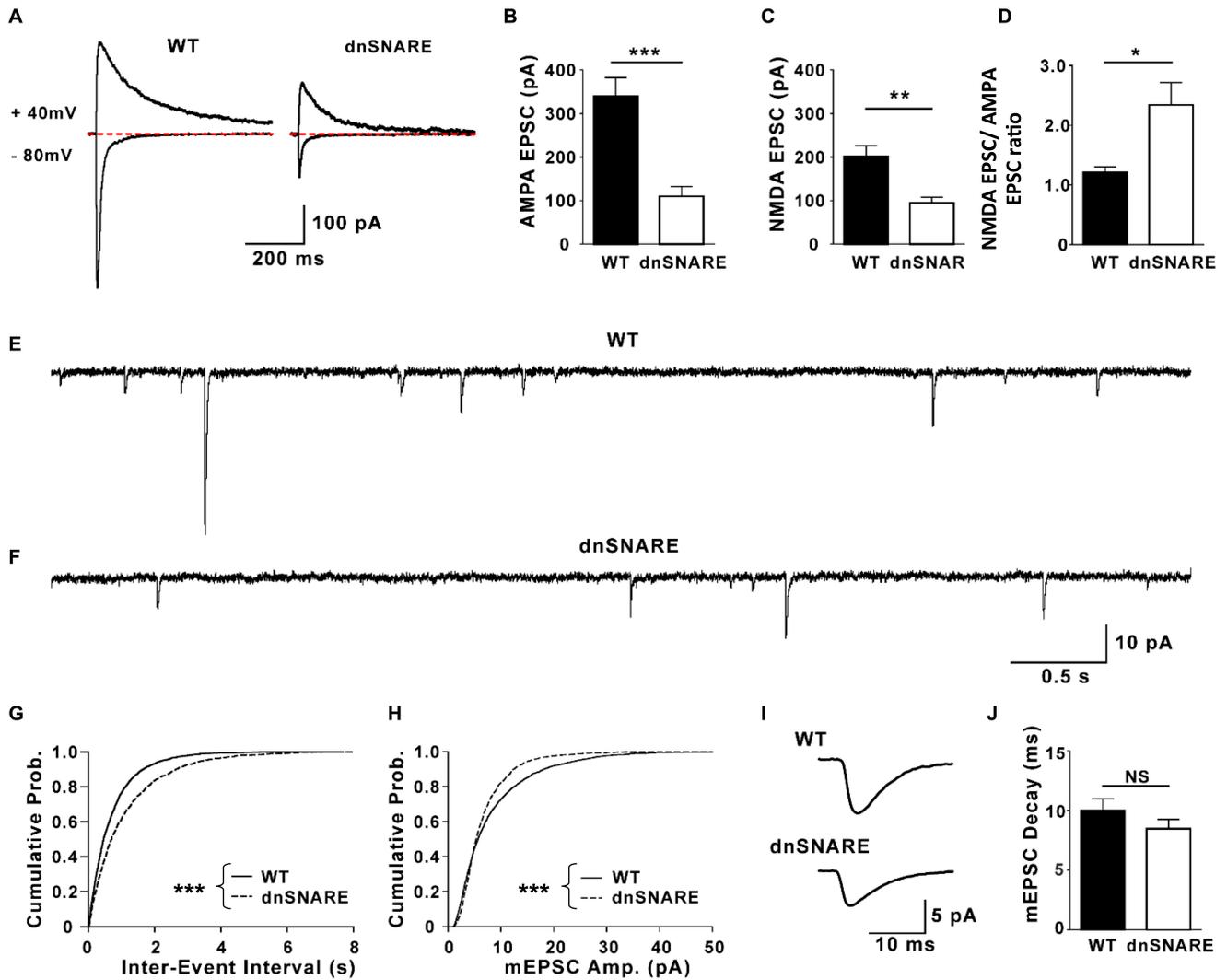**A** dnSNARE Mouse

Virus
CAG-mRFP1

Dox | Virus → Histology
0 → 30 dpi

B RFP / GFP / DAPI
dnSNARE

C RFP / GFP

D RFP / GFP   dnSNARE
Outside
Inside

E WT   Inside (dnSNARE)   Outside (dnSNARE)
Protrusions / μm
Cumulated dendritic length (μm)

F dnSNARE
Protrusions / μm
***
Outside   Inside

G dnSNARE
% of total protrusions
*   *
F   T   M

H
Decrease of protrusion density (%)
GFP+ astrocyte coverage (%)

I
Protrusions / μm
***
WT
tetO.dnSNARE
dnSNARE

J
% of total protrusions
**   **
F   T   M

K WT   dnSNARE

L
Number of intersections
**   *   *   ***   **   **   ***
Distance from the soma (%)
WT
tetO.dnSNARE
dnSNARE

M
Dendritic length (μm)
**   *
WT
tetO.dnSNARE
dnSNARE

N
Dendritic length (μm)
GFP+ astrocyte coverage (%)

O
Dox | BrdU → Histology → Histology
0   1   30 dpi

P Overlay   BrdU   Neu-N

Q
BrdU+ cells /DG
NS
1 dpi

R
Newborn neurons /DG
NS   ***
30 dpi
WT
tetO.dnSNARE
dnSNARE

Figure 3

A

B

C
GFP⁺ Astrocyte
Newborn Neuron
GFP⁻ Astrocyte
Presynaptic Bouton

Inside

Outside

E

NS

Ensheathed / total synaptic surface area (%)

25					
20					
15					
10					
5					
0					

Neuron GFP : + + - - + -
Astrocyte : in out in out
Mice: dnSNARE WT

D

Newborn neuron at 30 dpi (GFP+)	GFP⁻ neuron

dnSNARE Inside

dnSNARE Outside

WT

Figure 4

Figure 5

Figure 6

A

Dox

0   30 days

Microdialysis + HPLC

B

C

Hippocampal WT astrocytes

GFAP / GFP

Hippocampal dnSNARE astrocytes

GFAP / GFP

D

E

F

WT

dnSNARE

D-serine

D-serine

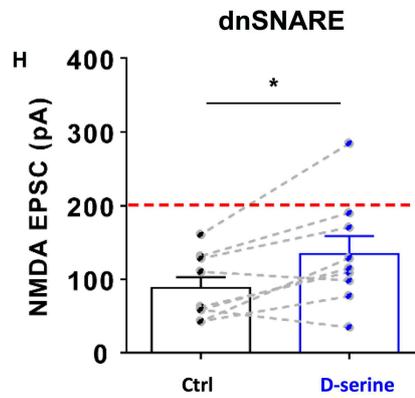50 pA
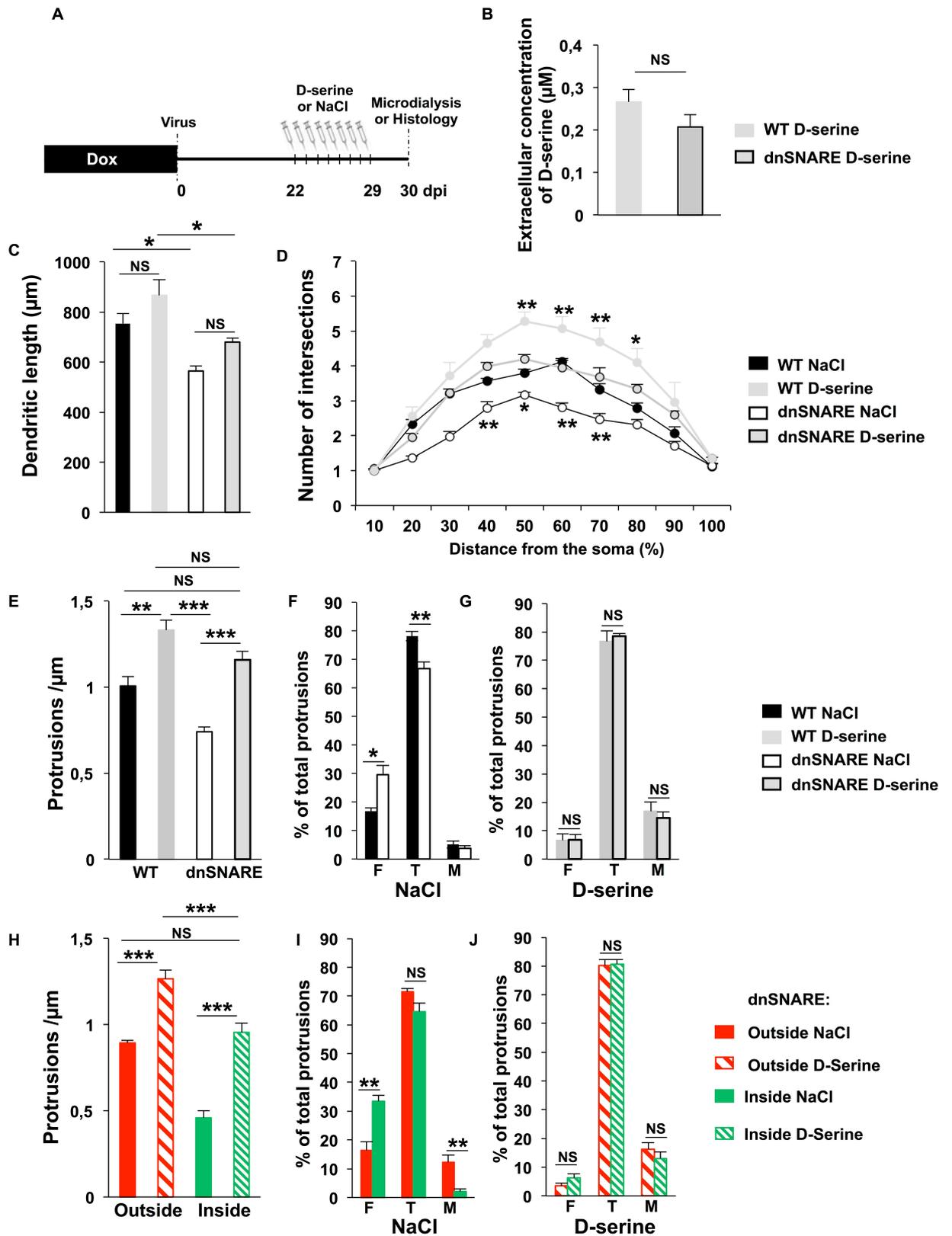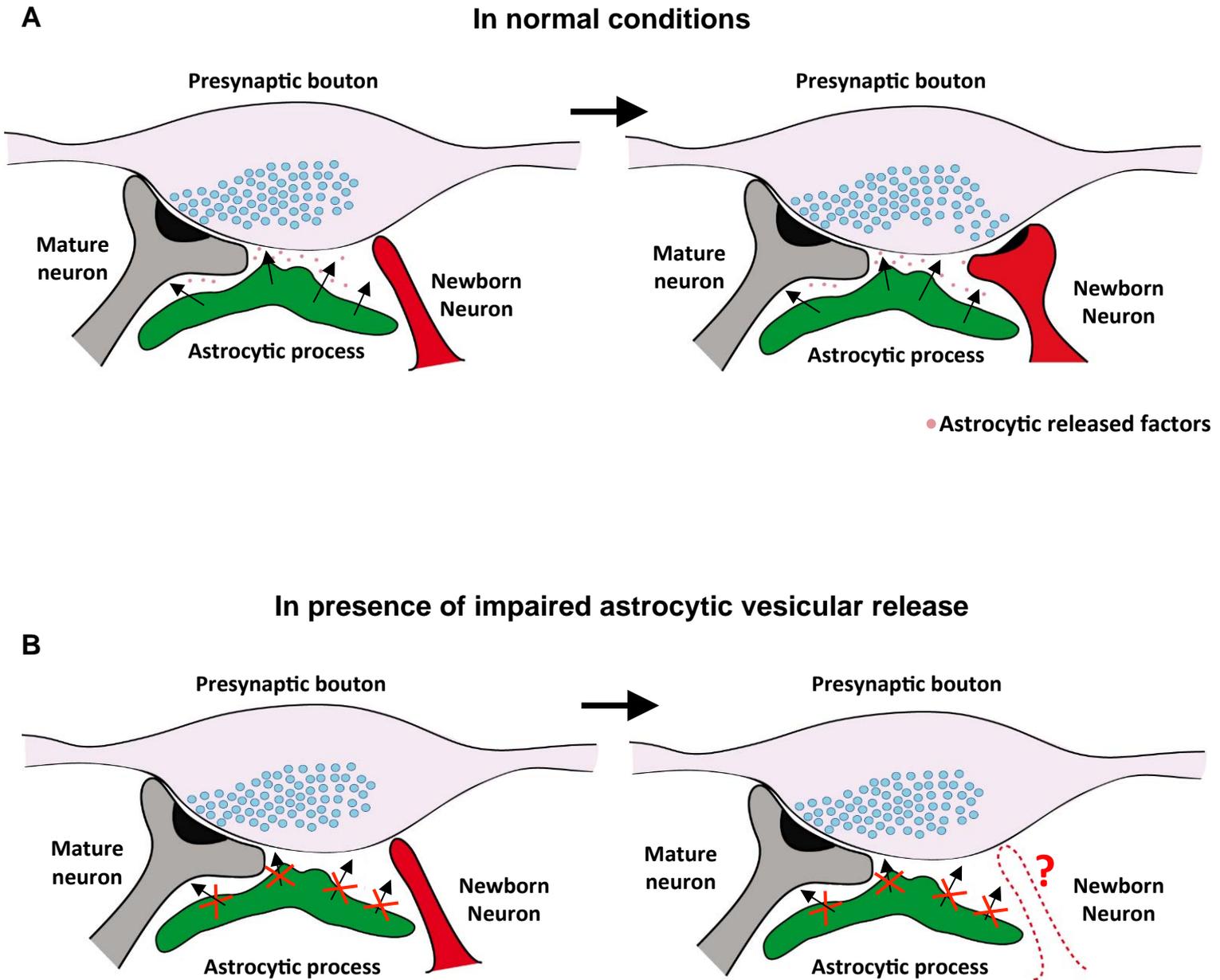
100 ms

+ 40mV

+ 40mV

G

WT

H

dnSNARE
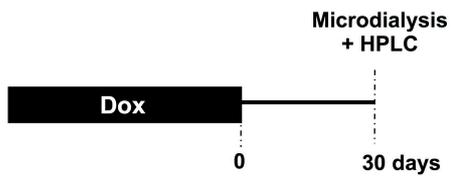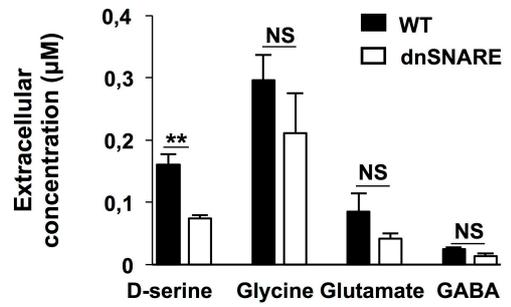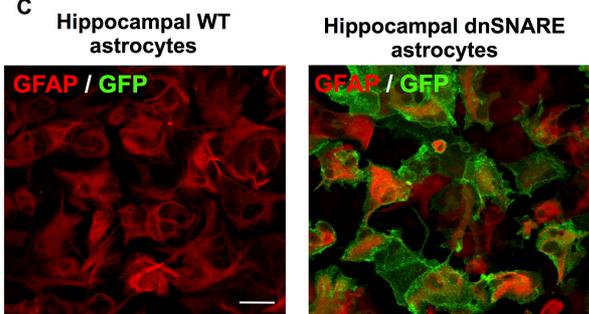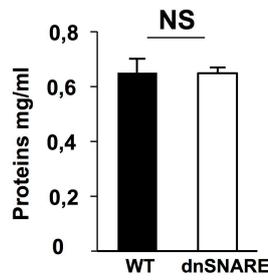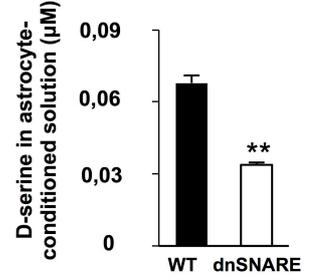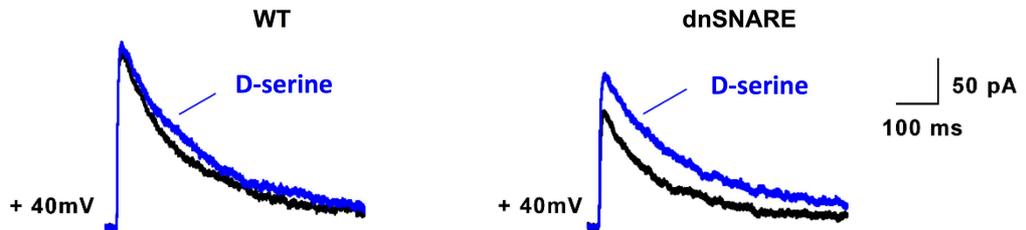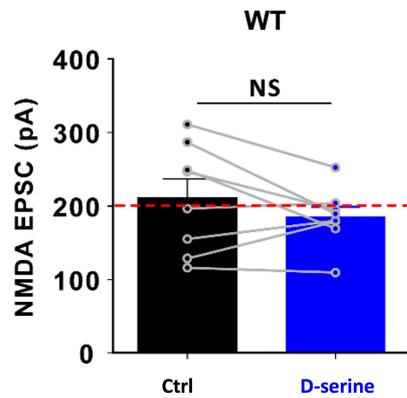
Figure 7

# Figure S1. Related to Figure 1.

Synaptic integration of new neurons

A   In normal conditions

**B**   In presence of impaired astrocytic vesicular release

Figure S1. Testing the role of astrocytic vesicular release in the synaptic integration of adult-born neurons
Schematic representation. (**A**) In the adult hippocampus newborn neurons extend dendritic protrusions (in red) which preferentially contact pre-existing axon terminals (presynaptic bouton, in purple), already synapsing with other dendritic spines (in grey), thereby forming multiple synapse boutons (MSB). Adult astrocytes form perisynaptic processes (in green) which are in close contact with MSB and release unknown factors (small dots in pink). (**B**) To test whether these astrocytes-released factors may be involved in the synaptic integration of new neurons, we used inducible genetic manipulations to block vesicular release from astrocytes during the critical period of synaptic maturation of identified cohorts of newborn neurons.

# Figure S2. Related to Figure 1.

iBot-Glast-CreER[T2] mouse

A

B

C

dnSNARE mouse

D

E

F

G

H

I

J
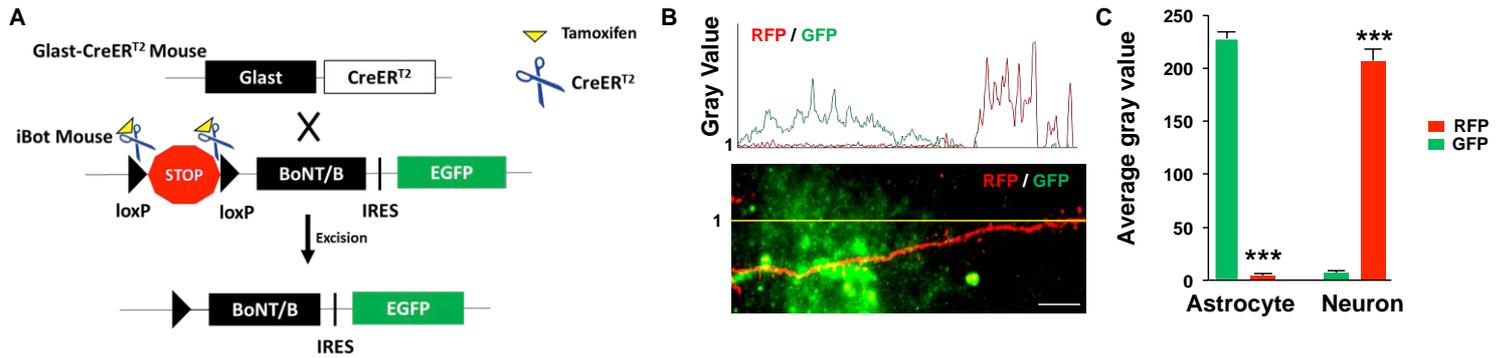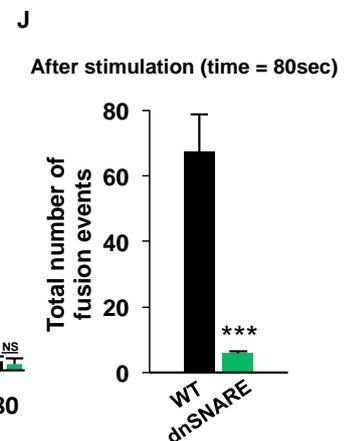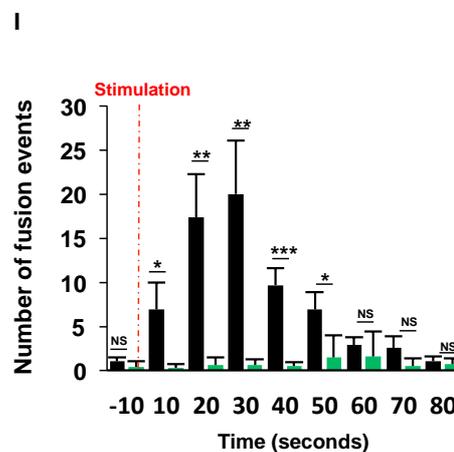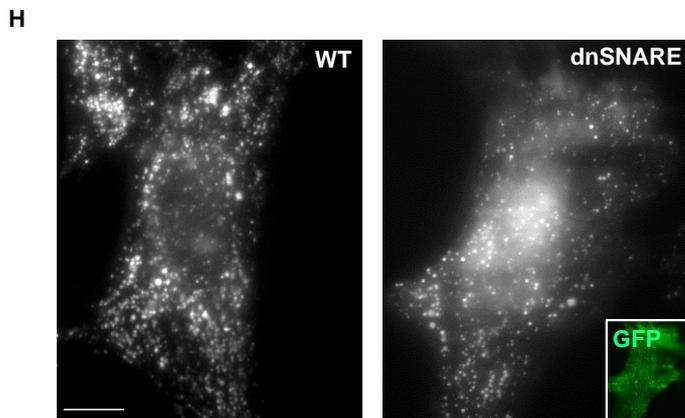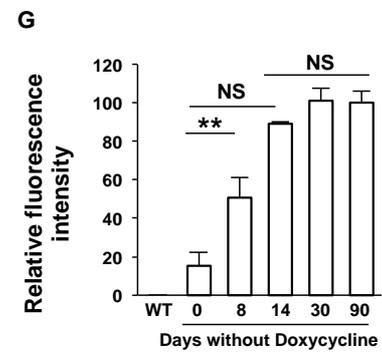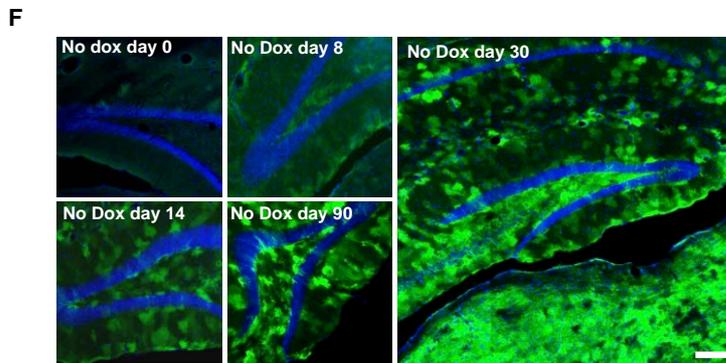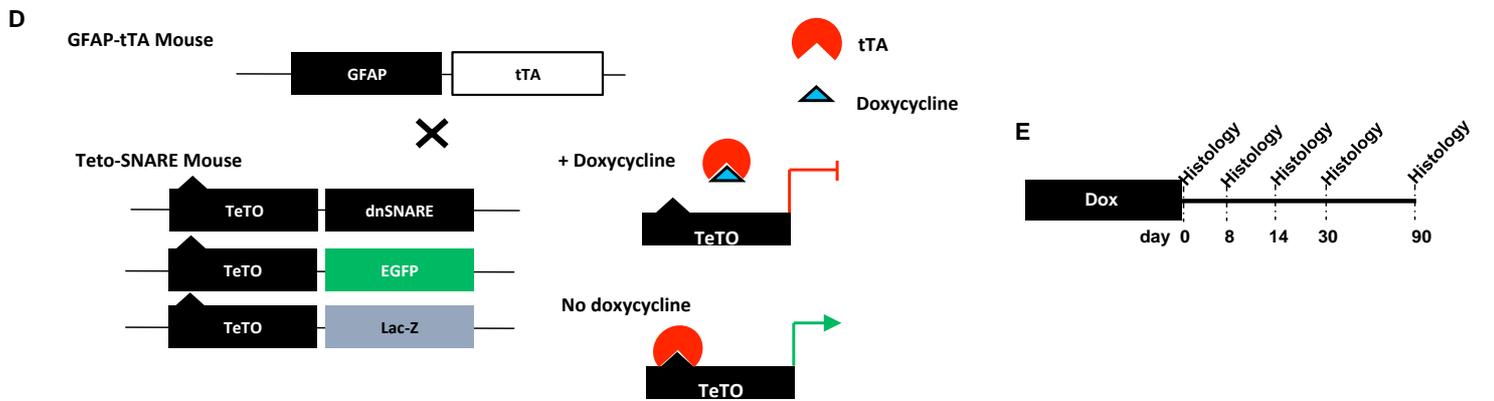
Figure S2. Transgene expression in astrocytes reduces vesicular release

(**A**) iBot-Glast-CreER^{T2} mouse. (**B**) Fluorescence intensity in the red and green channels along the yellow line (1) shown on the confocal micrograph below. Measurements are performed in newborn neurons (30 dpi) and GFP$^+$ astrocytes. Scale bar, 5µm. (**C**) Average maximal GFP and RFP fluorescence intensity measured in neurons and astrocytes as shown in B (nonparametric Kruskal–Wallis). (**D**) dnSNARE mouse. (**E**) Experimental timeline: Mice were fed with doxycycline-containing diet from mating on. Doxycycline was withdrawn at 8 weeks of age and mice were sacrificed 0, 8, 14, 30 or 90 days later. (**F**) Sample confocal micrographs of hippocampal sections of dnSNARE mice with time after doxycycline withdrawal. Scale bar, 100µm. (**G**) GFP fluorescence intensity with time after doxycycline removal (One-Way ANOVA, $F_{5,17}=18,8014$, P=0,0045 followed by post-hoc Tukey's HSD test). (**H**) Sample micrographs of WT and dnSNARE-expressing astrocytes in culture, loaded with acridine orange and before stimulation with ionomycin. Transgene expression in astrocytes was verified using GFP expression (right, inner panel). Scale bar 20µm. (**I**) Quantification of the number of fusion events over time (10 seconds bins) before and after stimulation with ionomycin application, using TIRF illumination (n=9 cells per group, Two-Way ANOVA with repeated measures F1,16 =27.02, P<0.0001 followed by post-hoc Tukey's HSD). (**J**) Average of the total fusion event during the first 80 seconds after ionomycin application in WT and GFP$^+$ astrocytes (n=9 cells, nonparametric Wilcoxon test). Values represent the mean ± s.e.m. NS: not significant, *P<0.05, **P<0.01, ***P<0.001.

Figure S3. Related to Figure 2.
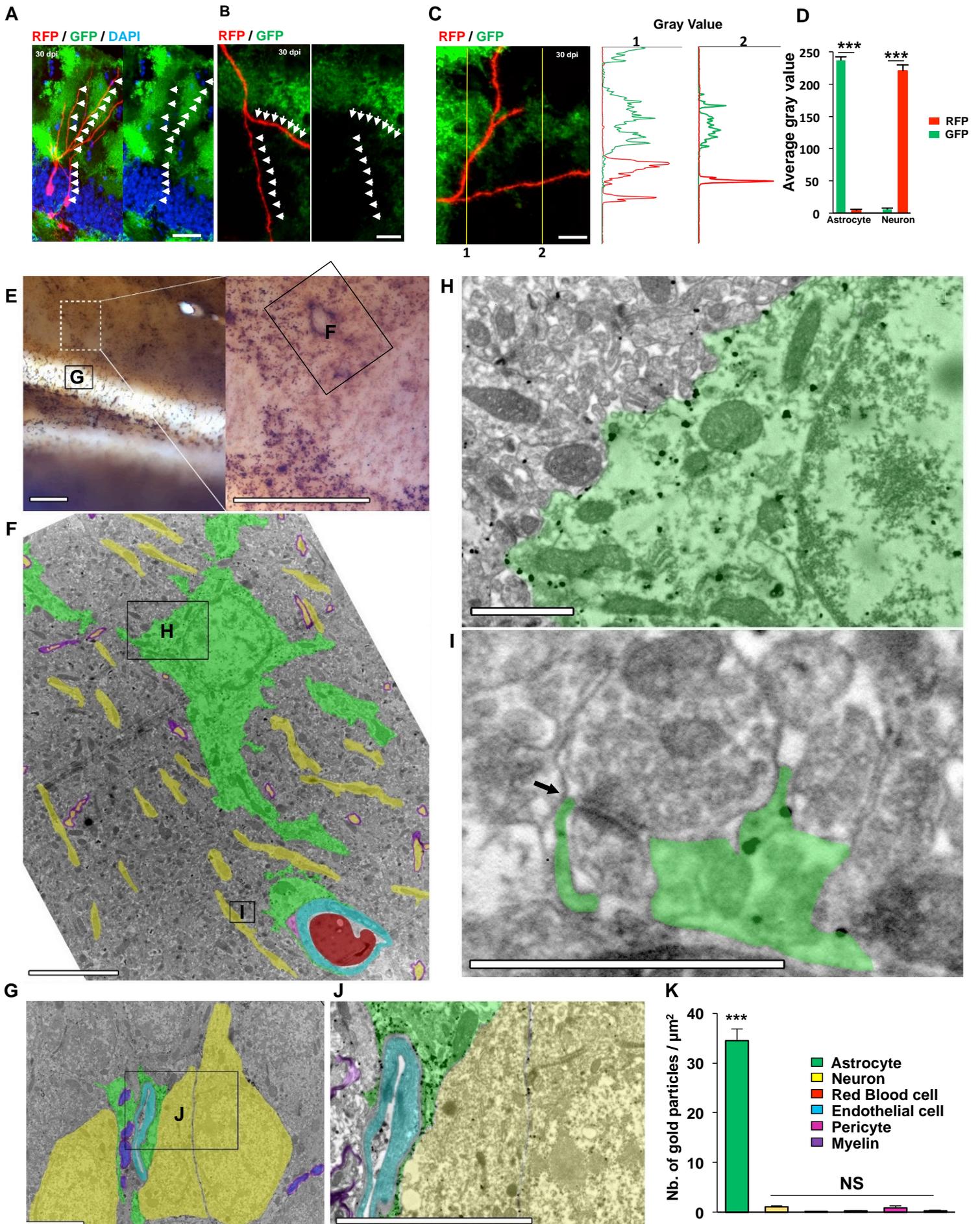
Figure S3. GFP is expressed in astrocytes of the molecular layer of the hippocampus of dnSNARE mice, but not in other cell types

(**A, B**) Confocal micrographs of 30 dpi RFP-expressing new neurons among GFP-expressing astrocytes. Right panels: Same image as on left panels, without the red channel, showing the absence of GFP expression in RFP$^+$ neurons. Arrows point to the position of the dendrites labeled in the left panels. Blue: DAPI, green: GFP, red: RFP. Scale bars: (**A**) 50μm; (**B**) 20μm. (**C**) Left panel: Fluorescence intensities were measured in the red and green channel along the lines **1** and **2** and the corresponding histograms are shown in the right panels. (**D**) Average GFP and RFP fluorescence maximal intensity measured in neurons and astrocytes (nonparametric Kruskal–Wallis test). (**E**) Hippocampal section of dnSNARE mouse showing, in the molecular layer of the dentate gyrus, a GFP-immunogold labeled astrocyte that was analyzed with electron microscopy. Boxed area in left panel is shown in right. Letters indicate the corresponding electron micrographs. (**F**) Electron micrograph of the astrocyte boxed in panel A, false-colored in green. In the same section: dendrites (yellow), axons (yellow) myelin (purple), endothelial cell (light blue), red blood cell (red) and a pericyte (pink). (**G**) Electron micrograph of the granule cell layer (boxed in panel E), showing neuronal somata (yellow), endothelial cell (light blue), astrocytic perisynaptic process (green), myelin (purple) and axons (dark blue). (**H**) Higher magnification view of the boxed area in F, showing the astrocytic soma. Note the black gold particles in the astrocyte. (**I**) Higher magnification of boxed area shown in F, showing a synapse (arrow) with perisynaptic processes (geen). (**J**) Higher magnification view of the area boxed in G, showing a neuronal soma and astrocytic perivascular process. (**K**) Density of gold particles per profile of each cell type analyzed (nonparametric Kruskal–Wallis test). Scale bars 50μm (**E**), 5μm (**F,G,J**), 1μm (**H,I**). Values represent the mean ± s.e.m. NS: P>0.05, ***P<0.0001.

Figure S4. Related to Figure 2.
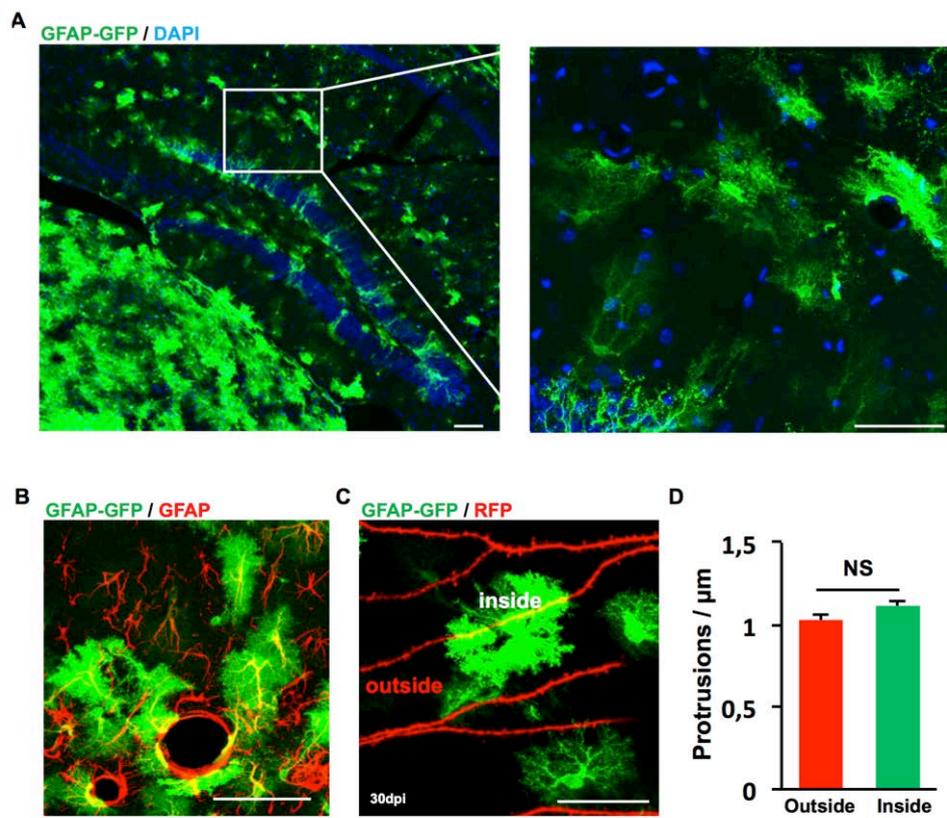
Figure S4. GFP expression in astrocytes does not alter dendritic protrusion density on adult-born neurons (**A**) Left panel: confocal micrograph of the dentate gyrus of a GFAP-GFP mouse. Right panel: higher magnification view of the boxed area. Scale bars, 50μm. (**B**) Confocal micrograph of the molecular layer of the dentate gyrus after GFAP immunostaining (red). $55 \pm 7\%$ of GFAP$^+$ cells also express GFP. Scale bar, 50μm. (**C**) Confocal micrograph of dendrites of newborn neurons (in red) at 30 dpi, intersecting with the territories of GFP$^+$ astrocytes. (**D**) Density of protrusions on dendritic segments intersecting (inside, green) and extending outside of GFP$^+$ astrocytes (n=3 mice per group, bilateral Student's t-test, NS: P>0.05). Values represent mean $\pm$ s.e.m.

Figure S5. Related to Figure 2.

A

BrdU or Virus · Histology

Dox

0 · 21 dpi

B

Protrusions / μm

Outside
Inside

C

% of total protrusions

F · T · M

D

Protrusions / μm

WT
dnSNARE

E

% of total protrusions

F · T · M

NS

F

RFP / GFP / DAPI

21 dpi

WT

dnSNARE

G

Dendritic length (μm)

NS

WT · dnSNARE

H

Number of intersections

Sholl Analysis

● WT
○ dnSNARE

NS

Distance from the soma (%)

I

New neurons / DG
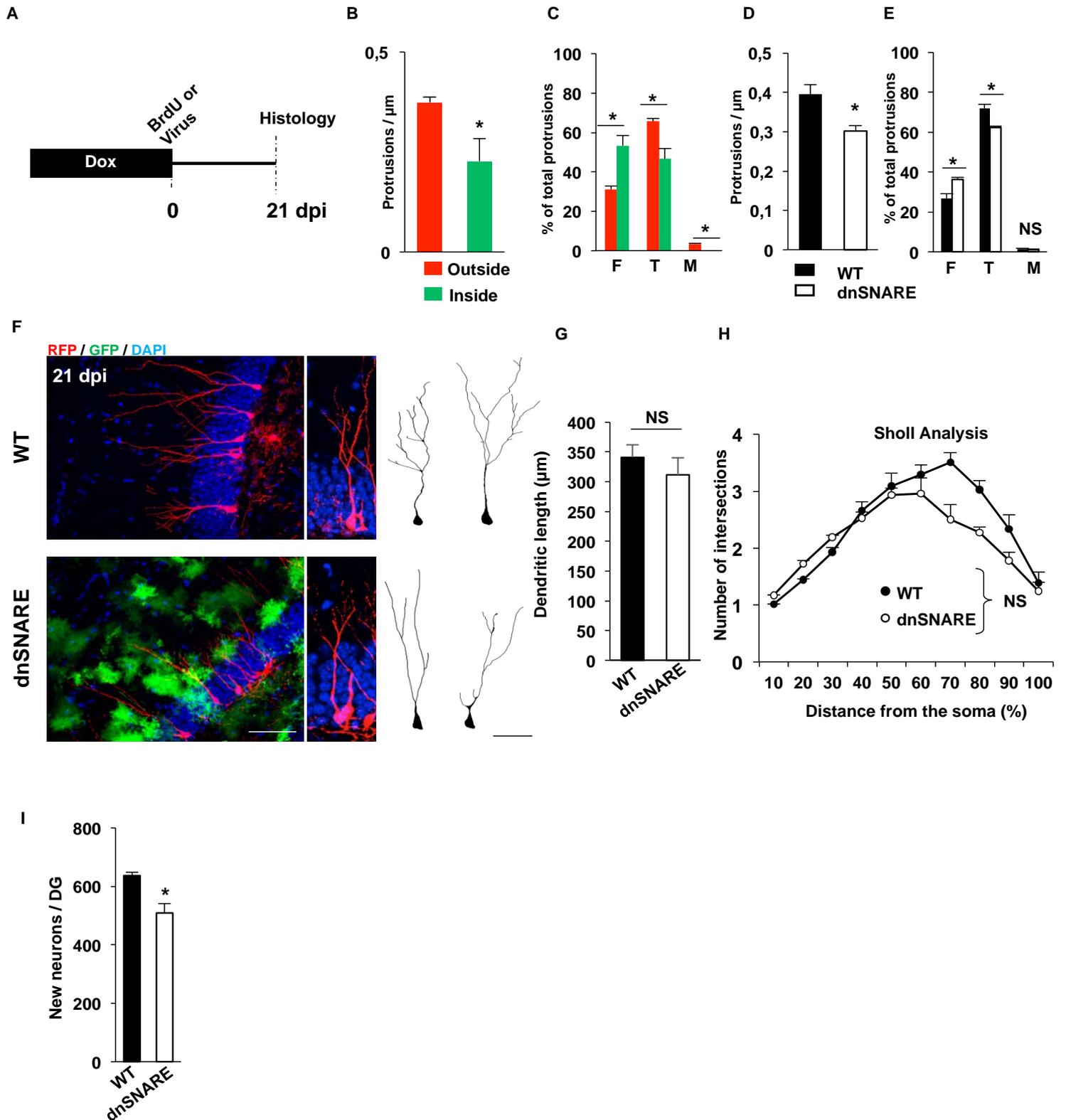
WT · dnSNARE
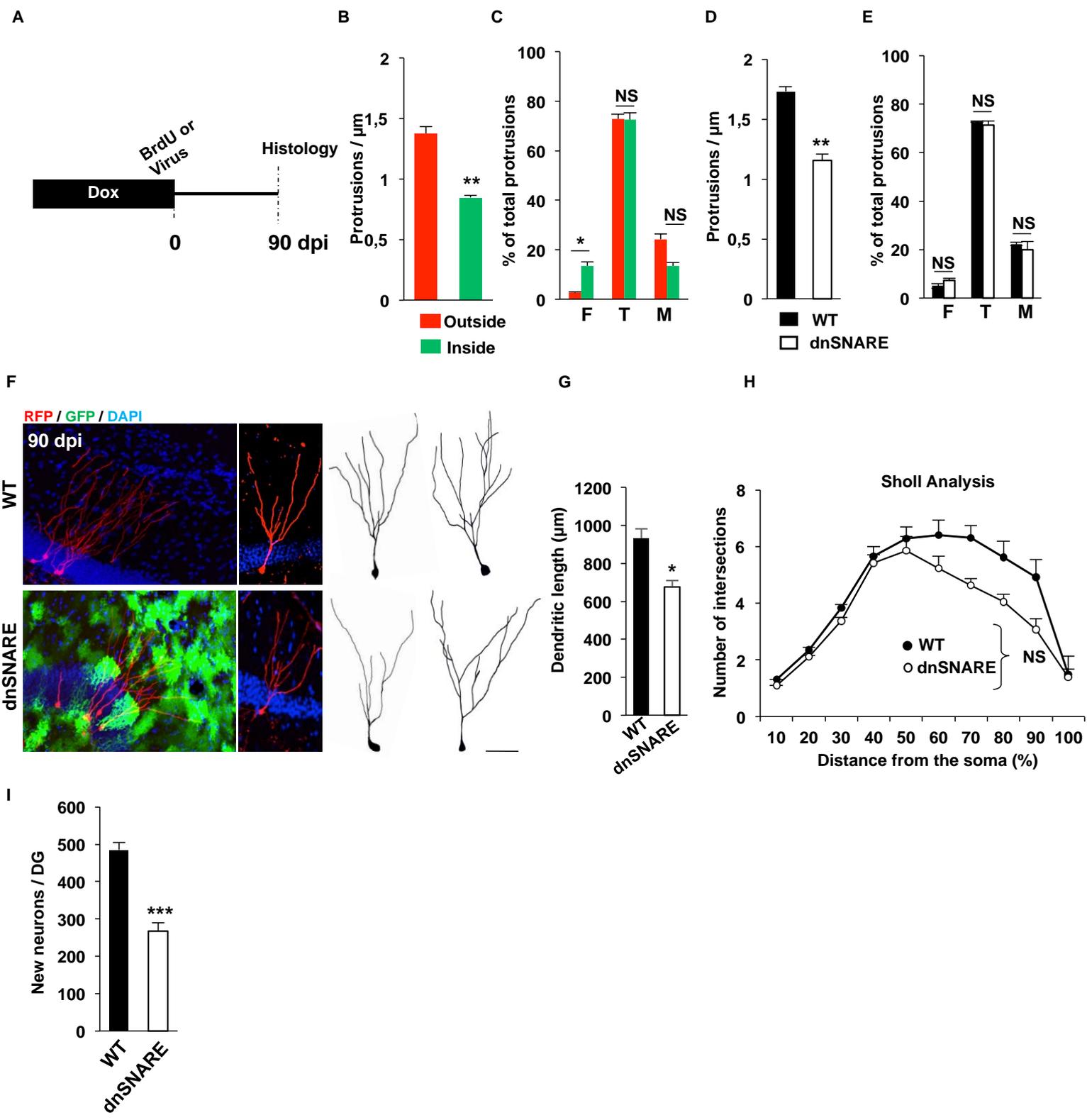
Figure S5. dnSNARE expression in astrocytes impairs the maturation and survival of new neurons at 21 dpi

(**A**) Experimental design: Mice were injected either with RFP-expressing Moloney virus or BrdU (100 mg/kg, 3 injections IP with 2 hours intervals). Doxycycline was withdrawn immediately thereafter and hippocampal slices were analyzed at 21 dpi. (**B**) Density of protrusions on new neurons dendrites intersecting transgene-expressing astrocytes (inside) and extending out of them (outside) (bilateral Student's t-test, *P<0.05). (**C**) Proportion of dendritic protrusions with filopodia (F), thin (T) and mushroom (M) morphology in the dendritic segments intersecting transgene-expressing astrocytes (bilateral Student's t-test between category). (**D**) Global density of dendritic protrusions on new neurons in dnSNARE mice as compared to WT mice (bilateral Student's t-test). (**E**) Global proportion of protrusions with different morphologies in new neurons in dnSNARE mice as compared to WT mice (filopodia (F), thin (T) bilateral Student's t-test; mushroom (M) Mann-Whitney,). (**F**) Left panels: Confocal micrographs of RFP$^+$ new neurons. Scale bar, 50μm. Middle panels: higher magnification confocal micrographs of new neurons. Right panels: 3D reconstructions of new neurons. Scale bar, 20μm. (**G**) Total dendritic length (bilateral Student's t-test). (**H**) Sholl analysis of the dendritic complexity of new neurons: (Two-Way ANOVA with repeated measures $F_{1,6}$ =1.46, P=0.2710). (**I**) Number of newborn neurons (co-expressing BrdU and Neu-N) in the DG (bilateral Student's t-test,). Values represent the mean ± s.e.m. NS: not significant, *P<0.05.

Figure S6. Related to Figure 2.

A

Dox — BrdU or Virus — Histology

0 — 90 dpi

B

Protrusions / μm — Outside, Inside — **

C

% of total protrusions — F (*), T (NS), M (NS)

D

Protrusions / μm — WT, dnSNARE — **

E

% of total protrusions — F (NS), T (NS), M (NS)

F

RFP / GFP / DAPI

90 dpi

WT

dnSNARE

G

Dendritic length (μm) — WT, dnSNARE — *

H

Sholl Analysis

Number of intersections vs Distance from the soma (%)

WT, dnSNARE — NS

I

New neurons / DG — WT, dnSNARE — ***

Figure S6. dnSNARE expression in astrocytes induces long-lasting inhibition of adult-born neuron maturation and survival at 90 dpi

(**A**) Experimental design: At day 0, all mice were injected either with a retrovirus (n=3 mice per group) or with BrdU (100 mg/kg, 3 injections IP with 2 hours intervals, n=5 mice per group). Doxycycline was withdrawn immediately thereafter and hippocampal slices were analyzed at 90 dpi. (**B**) Protrusions density on dendrites intersecting (inside) transgene-expressing astrocytes and extending out of them (outside) (bilateral Student's t-test). (**C**) Proportion of dendritic protrusions with different morphologies (filopodia (F) Mann-Whitney,; thin (T) and mushroom (M) bilateral Student's t-test). (**D**) Global density of dendritic protrusions (bilateral Student's t-test). (**E**) Global proportion of protrusions with different morphologies (bilateral Student's t-test). (**F**) Left panels: Confocal micrographs of RFP$^+$ new neurons. Scale bar, 50µm. Middle panels: higher magnification of new neurons. Right panels: confocal 3D reconstructions. Scale bar, 20 µm. (**G**) Dendritic length of new neurons (bilateral Student's t-test). (**H**) Sholl analysis of the dendritic complexity (Two-Way ANOVA with repeated measures $F_{1,4}$ =2.7947, P=0.1699). (**I**) Number of new neurons (co-expressing BrdU and Neu-N) in the DG at 90 dpi. (bilateral Student t-test). Values represent the mean ± s.e.m. NS: not significant, *P<0.05, **P<0.01, ***P<0.001.
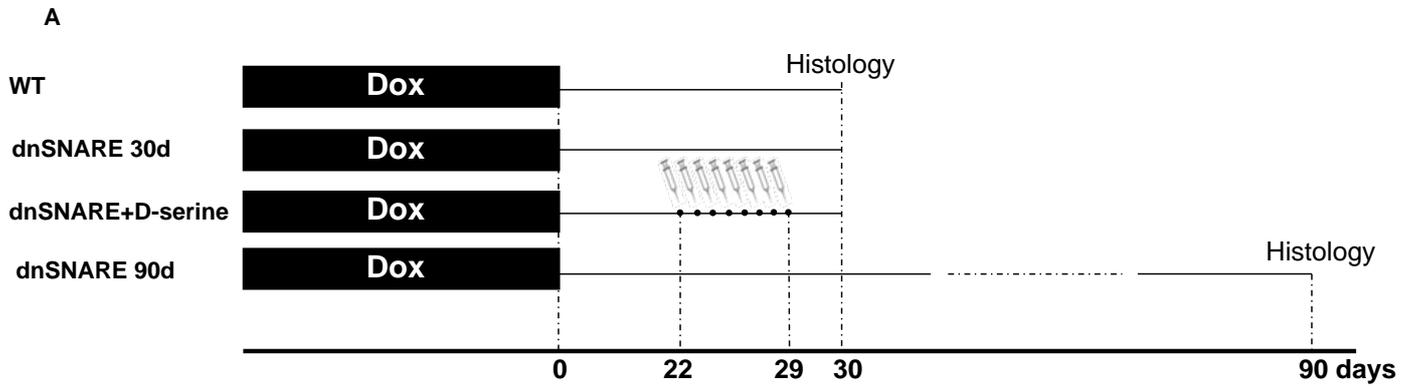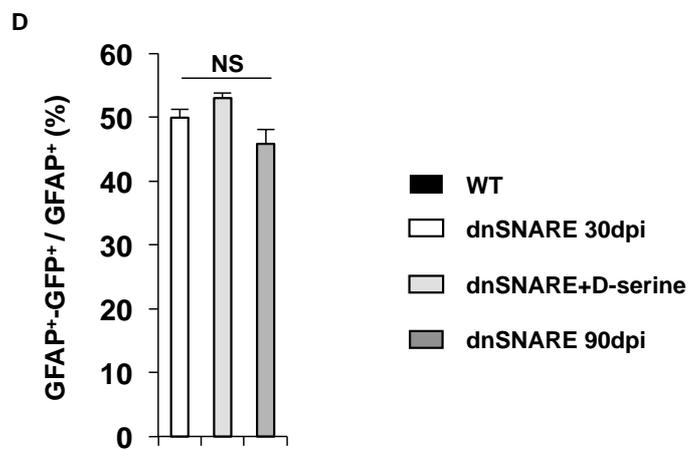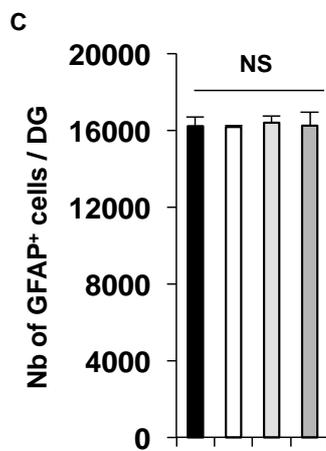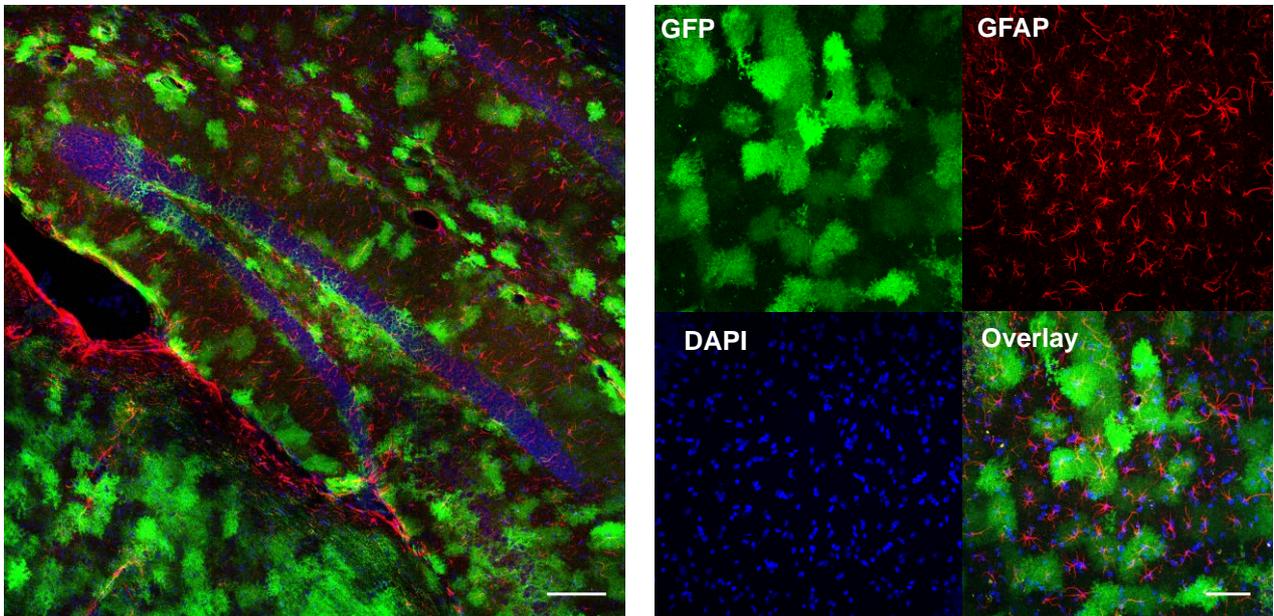
Figure S7. Related to Figure 7.

A

B GFAP / GFP / DAPI

Figure S7. The numbers of GFAP-immunolabeled astrocytes or of transgene-expressing astrocytes are not changed in the different experimental conditions

(**A**) Experimental timeline: WT and dnSNARE mice were kept under Doxycycline (Dox) until 8 weeks of age. One group of WT and of dnSNARE mice was not treated. One group of dnSNARE mice received daily injections of D-serine from 22 to 29 days after Dox withdrawal. These three groups were analyzed 30 days after Dox removal. One group of dnSNARE mice was analyzed at 90 days (n=3 mice per group). (**B**) Left panel: confocal micrograph of a hippocampal section of a dnSNARE mouse, immunostained for GFAP (in red), 30 days after Dox withdrawal. Scale bar, 100 μm. Right panel: Higher magnification confocal micrograph of the molecular layer showing GFP, GFAP, DAPI and overlay. Scale bar: 50μm. (**C**) The number of GFAP+ cells in the dentate gyrus was similar between experimental groups (Welch Anova $F_{3,3.53}=0.0576$, P=0.9792). (**D**) The proportion of GFAP+ cells that co-expressed GFP was unchanged between groups (One-Way ANOVA $F_{2,8}=3.56$, P=0.0953). Values represent the mean ± s.e.m. NS, not significant.

Supplemental Experimental Procedures

Experimental animals:

All procedures were conducted in strict accordance with the Swiss animal experimentation authorities (Service de la consommation et des affaires vétérinaires, Chemin des Boveresses 155, 1066 Epalinges, Switzerland, permit number: 2302.2). Every effort was made to minimize the number of animals used and their suffering. All mice were housed in standard cages under a 12-h light/dark cycle and temperature-controlled (22°C) conditions. Food and water were available *ad libitum*. Animals used for the study were adult mice of 8 to 10 weeks of age at the beginning of the experiment. dnSNARE mice (kind gift of P. Haydon, Tufts University, Boston, USA), were generated by crossing **1)** the GFAP-tTA line expressing the tet-off tetracycline transactivator under the control of the GFAP promoter and **2)** the tetO.dnSNARE line containing a tet-operator-regulated dominant-negative soluble N-ethylmaleimide-sensitive factor attachment protein receptor (dnSNARE) domain of synaptobrevin 2 as well as the reporter genes lacZ and GFP (Pascual et al., 2005). Doxycycline (Dox) was administered in the food pellets (40-ppm, Harlan Laboratory Wi, USA) of dnSNARE and control animals (WT and tetO.dnSNARE littermate) starting from mating of the parental pair onwards and the discontinuation of dox treatment in adult mice resulted in a slow increase in transgene expression that reached a plateau after 2 weeks, as monitored by GFP fluorescence intensity (Figure S2E-G). This design was previously shown to prevent transgene expression during embryonic development and to prevent expression in non-astrocytic cell types (Fellin et al., 2009; Halassa et al., 2009; Pascual et al., 2005).

Since doxycycline has an effect on adult neurogenesis (Sultan et al., 2013) all controls received the same dox treatment as dnSNARE mice, to avoid the confounding effect of dox on adult neurogenesis.

dnSNARE and control mice (wild-type (WT) and monogenic) were chronically treated with dox and injected, at 8 weeks of age, with the cell proliferation marker 5-Bromo-2-deoxyuridine or the Moloney murine leukemia virus (MoMuLv) carrying the expression cassette for RFP. Doxycycline was removed immediately after the last injection and analyzes were performed at 1, 21, 30 and 90 days post injection (dpi). This experimental design enabled the BrdU/MoMuLv labeled cells to proliferate in absence of transgene expression, but to differentiate and mature in presence of an increasing expression of dnSNARE in astrocytes. The experimental groups were distributed as follows:

Mice analyzed at 14 dpi, injected with BrdU: dnSNARE n=3, WT n=3

Mice analyzed at 21 dpi, dnSNARE n=3, WT n=5

Mice analyzed at 30 dpi, injected with BrdU: dnSNARE n=5, tetO.dnSNARE n=5, WT n=5

Mice analyzed at 30 dpi, injected with the retrovirus: dnSNARE n=6, tetO.dnSNARE n=3, WT n=6

Mice analyzed at 90 dpi, dnSNARE n=3, WT n=3

Mice analyzed for microdialysis, WT NaCl n=6 WT D-serine n=5, dnSNARE NaCl n=5 and dnSNARE D-serine n=5.

Mice analyzed for D-Serine experiment, WT NaCl n=4 WT D-serine n=4, dnSNARE NaCl n=5 and dnSNARE D-serine n=5.

Control groups were littermate animals

iBot-Glast-CreER^{T2} mice were obtained by crossing 2 lines of transgenic mice (Slezak et al., 2012) : **1**) the iBot line, that contains a CAG (cytomegalovirus early enhancer and chicken beta-actin) promoter, a floxed-STOP cassette upstream of the gene encoding the *Clostridium botulinum* neurotoxin serotype B light chain (BoNT/B) followed by an GFP and **2**) the Glast-CreER^{T2} T45-72 line in which the expression of tamoxifen-inducible Cre recombinase (CreER^{T2}) is under the control of the astrocyte-specific promoter GLAST.

Mice were injected with BrdU, followed one day later by a stereotaxic injection of RFP-encoding MoMuLv to label newborn cells. To induce Cre recombinase activity and activate BoNT/B expression, mice were injected with 2mg of tamoxifen (Tam, stock 20mg/mL in sterilized corn oil, Sigma). Control littermate animals were injected either with tamoxifen or with sterilized corn oil. Tamoxifen was injected intraperitoneally (i.p.) for 5 consecutive days, during the maturation period of the newly formed, labeled neurons (daily injections between day 7 and 11 after viral injection (Tashiro et al., 2007) and hippocampal slices were analyzed at 30 dpi.

The experimental groups were distributed as follows:

iBot-Glast-CreER^{T2} injected with tamoxifen n=5

Control mice injected with tamoxifen: n=3 monogenic iBot and n=2 WT littermate

Control mice injected with vehicle (oil): n=2 monogenic iBot and n=1 WT littermate

GFAP-GFP mice were a kind gift from the laboratory of Helmut Kettenmann (Max-Delbruck center, Berlin, Germany) (Nolte et al., 2001). They express GFP under the control of the astrocyte-specific GFAP promoter.

Experimental group: n=3 mice

D-Serine administration:

D-serine was prepared fresh every day and diluted in water + 0.9% NaCl. Mice were injected i.p. every day with 50 mg/kg of D-serine (Sigma-Aldrich) for 8 consecutive days or with vehicle (0.9% NaCl in sterilized water).

Stereotaxic viral injections:

Dividing neuronal progenitor cells and their progenies we identified and stably labeled using a MoMuLv encoding RFP or GFP under the control of the CAG promoter (Zhao et al., 2006). Viral injection was performed as previously described (Sultan et al., 2013). Briefly, mice were anesthetized with a mixture of 90 mg/kg ketamine and 4.5 mg/kg xylazine (i.p.) and placed in a stereotaxic frame (Narishige Scientific Instruments, Tokyo, Japan). 1.5 ul of retroviral vector (final titer 10E8 pfu/ml) was injected in the dentate gyrus (Bregma: -2 mm anteroposterior, 1,75 mm lateral and -2,00 mm dorsoventral) using a calibrated 5µl Hamilton syringe fitted with a 33-gauge needle.

BrdU administration and tissue preparation:

Bromodeoxyuridine (BrdU, Sigma-Aldrich, Buchs, Switzerland) was injected i.p. at doses of 100 mg/kg in saline, 3 times at 2 hour intervals. 24 hours, 21 days, 14 days, 30 days or 90 days after the last injection, mice were deeply anesthetized with a lethal dose of pentobarbital (10mL/kg, Sigma-Aldrich, Buchs, Switzerland) and perfusion-fixed with 50 ml of 0.9% saline followed by 100mL of 4% paraformaldehyde dissolved in phosphate buffered saline (PBS 0.1M, pH 7.4). Brains were then removed, postfixed overnight at 4°C, cryoprotected 24h in 30% sucrose, rapidly frozen and sectioned at a thickness of 40 µm with a microtome-cryostat (Leica MC 3050S). Slices were then treated with formic acid (formamide 50% in 2X SSC buffer; 2X SSC is 0.3 M NaCl and 0.03 M sodium citrate, pH 7.0) at 65°c for 2 hours followed by DNA denaturation in 2 M HCl for 30 min at 37°C and rinsed in 0.1 M borate buffer pH 8.5 for 10 min.

Immunohistochemistry:

Non-specific antibody binding was blocked with 15% normal serum and 0.25% Triton-X100 in PBS 0.1M. Slices were then incubated for 40 hours at 4°C with the primary antibodies and 2 hours with the corresponding secondary antibodies: RFP signal was amplified using rabbit anti-RFP igG (Rockland Immunochemicals, Gilbertsville, Pennsylvania, USA; diluted 1:1000 in phosphate buffered saline) and Hylite 594 goat anti-rabbit IgG secondary antibody (Biotrend Chemicals AG, Wangen, Switzerland;1:500). GFP signal was amplified using Chicken anti-GFP IgG (Aves Labs,Tigard, Oregon, USA; 1:1000) and Dylight 488 goat anti-chicken IgY (Jackson ImmunoResearch Europe Ltd., Suffolk, United Kingdom; 1:500). BrdU was detected using rat anti-BrdU IgG (Abcam, Cambridge, United Kingdom; 1:200) and goat Alexa fluor 594 anti-rat IgG (Life Technologies Europe B.V., Zug, Switzerland; 1:250). Neu-N was detected using mouse anti-Neu-N IgG (Chemicon international 1:1000) and goat anti-mouse Alexa fluor 488 (Life Technologies Europe B.V., Zug, Switzerland; 1:250). GFAP was detected using rabbit anti-GFAP IgG (LifeTechnologies Europe B.V.; 1:500) and goat Alexa fluor 594 anti-rabbit. Nuclei were detected using the 4,6 diamidino-2-phenylindole (DAPI) nuclear stain.

DiI labeling:

30 days after the end of doxycycline treatment, dnSNARE and WT littermate mice were perfused with a 4% paraformaldehyde solution in PBS. Brains were removed, postfixed for 4 hours and then sectioned at a thickness of 50 um using a vibratome (Leica, VT100S). Dendrites of granule cells in the molecular layer of the dentate gyrus (DG) of both hemispheres were randomly labeled by adding a droplet of the liposoluble vibrant DiI cell-labeling solution (LifeTechnologies Europe B.V.) to the slice.

Confocal microscopy and image analysis:

All images were acquired using a confocal microscope (Zeiss LSM 710 Quasar Carl Zeiss, Oberkochen, Germany). BrdU- and GFAP-expressing cell densities were measured using stereology, as previously described (Sultan et al., 2013; Thuret et al., 2009). For each animal, all cells were counted in the entire thickness of the sections in a 1-in-6 series of sections (240 μm apart) with a 40× objective and the number of cells was then related to the granule cell layer volume and multiplied by the reference volume to estimate the total number of immunolabeled cells. The granule cell reference volume was determined by multiplying the area of the granule cell layer measured in a 1-in-6 series of sections between −1.3 and −2.9

mm from the Bregma stained with the nucleus marker DAPI using Axiovision© (Zeiss, Germany) software, by the distance between the sections sampled (240 μm). Cells expressing BrdU were counted in the granule cell layer and subgranular zone, whereas cells expressing GFAP were counted in the whole DG. For all experiments, the volume of the granule cell layer of all mice was measured. No change in hippocampal volume was found between experimental groups and their controls.

BrdU colocalization with the neuronal marker Neu-N (as well as GFAP colocalization with GFP) was examined using confocal microscopy and colocalization was confirmed on single optical sections, for 50-60 cells per animal. The proportion of double-labeled cells was then obtained for each animal and then averaged for each group.

Newborn neuron morphological analysis:

Dendritic arborization was measured for 25-30 newborn neurons per mouse, traced using Neurolucida© software and analyzed using Sholl analysis. The results were then normalized to the maximal length of the neurons.

Dendritic spine density and spine morphology was assessed as previously described (Sultan et al., 2013; Toni et al., 2007). Dendrites were imaged with confocal microscopy in the second third of the molecular layer and their length as well as their number of spines was measured using Image-J software, for 30-40 neurons per mouse. Spine density is expressed as the number of spines divided by dendritic length. Dendritic protrusions were classed in 3 groups based on the maximal diameter of their tips, as measured on maximal projections with Image-J: Filopodia (F) < 0.25μm, thin spines (T) 0.25 to 0.60 μm and mushroom spines (M) > 0.6 μm. The percentage of each type of dendritic protrusion was then expressed by neuron and averaged for each mouse (25 to 30 neurons per group, about 1000 protrusions per group).

To examine dendritic segments crossing the territories of GFP-expressing astrocytes, confocal stacks were reconstructed in 3D using IMARIS© software. The identity of the astrocytic territory crossed by dendritic segments was assessed on individual optical sections.

Electron microscopy:

dnSNARE mice were virally infected at seven weeks of age, then perfuse-fixed 30 days later and 50 μm thick coronal sections were collected. Epifluorescence microscopy was used to select sections showing clear intersections between GFP-positive newborn neuron dendrites and GFP-positive dnSNARE astrocytes. Selected sections were cryoprotected, freeze-thawed, blocked and then incubated in a rabbit anti-GFP primary antibody (overnight; 1:1000;

Invitrogen) and subsequently a biotinylated goat anti-rabbit secondary antibody (2 h; 1:200; Jackson Laboratories). Incubation in avidin-biotin-peroxidase complex (90 min; ABC Elite; Vector Laboratories) was followed by a reaction with 3,3-diaminobenzidine (DAB) and hydrogen peroxide (6 min; Vector Laboratories Kit). Sections were then post-fixed in 1% osmium tetroxide (30 min; Electron Microscopy Services), dehydrated in ascending concentrations of ethanol (50%; 70% with 1% uranyl acetate; 95% and 100%) and acetone, before being placed in resin overnight (Durcupan ACM Fluka, Sigma). They were then lifted onto glass slides, coverslipped and baked at 65°C for 72 h.

For immunogold labelling of GFP$^+$ dnSNARE astrocytes, the same primary antibody was used. This was followed by a 2 h incubation in a secondary goat anti-rabbit gold-conjugated antibody (1.4 nm colloidal gold; 1:100; Nanoprobes) and silver intensification of the gold particles (1 ml silver reagent; 2-4 min; HQ Silver kit, Nanoprobes) in 0.1 M sodium acetate 3-hydrate (Sigma). Sections were post-fixed in 1% osmium tetroxide for 8 min then dehydrated and embedded in resin as above.

The points of intersection identified with epifluorescence microscopy were labelled with dark DAB peroxidase precipitate and could be captured in greater detail using light microscopy (LM; 100× magnification; Axiovision©). The best candidates for electron microscopic (EM) analysis were cut from the slides, re-embedded on blocks, trimmed and then sectioned at 50-70 nm thickness using a Reichert-Jung ultramicrotome. Serial sections were collected onto formvar-coated, single-slot, copper grids and contrasted with lead citrate (Electron Microscopy Services) before examination on a Philips CM10 electron microscope. Serial section images of a newborn neuron dendrite, labeled with a dense DAB-peroxidase precipitate, were captured to show its relationship with the processes of dnSNARE astrocytes. Processes of the dnSNARE astrocyte were identified by their dark-labelled membranes or gold particles at high magnification and their connections to astrocytic cell bodies and characteristic wrappings of blood vessels at lower magnifications. Synaptic contacts were defined by the presence of presynaptic vesicles accumulation, a clearly-defined synaptic cleft, cleft material and a postsynaptic density.

The newborn neuron dendrites and dnSNARE astrocytes were reconstructed in 3D using Fiji Image-J software and images were prepared using Photoshop© and Illustrator© software (Adobe). Tissue from virus-injected, control mouse brains was processed and examined in a similar fashion to investigate the relationships between a newborn neuron dendrite and unlabeled wild-type astrocytes. Newborn neurons dendritic spines inside and outside the territory of a dnSNARE astrocyte were assessed for their relationship with astrocytic

processes, as were newborn neuron spines in wild-type tissue. For comparison, GFP⁻ (putatively mature neuron) spines were assessed in similar regions (middle third of the molecular layer) of similar tissue. The proportions of perisynaptic surfaces apposed by astrocytic astrocytic processes were assessed by measuring the perimeters of synapse-forming axonal boutons and spines (in all serial EM sections they appeared in) and the proportion of these perimeters apposed by astrocytes.

The volumes of dendritic spines were measured for reconstructed newborn neuron dendrites in both control and dnSNARE mice, as were those of randomly-selected, GFP⁻, morphologically mature dendrites in the same tissue (Fiji Image-J software). Unbiased stereological assessment of synapse density was performed as described previously (Sterio, 1984). Synapse density was determined by systematic random sampling on 60 dissector pairs in each area, using the postsynaptic density as counting unit.

Electrophysiology:

Transverse 300-μm-thick slices were cut with a Leica VT-1200 vibroslicer from the hippocampus of 11-12-week-old dnSNARE or WT mice corresponding to 30 days after viral injection. Animals were decapitated after anesthetization with 3% Isoflurane. Slices were kept at 35°C for 30 min after slicing and then at room temperature. For the dissection and storage of slices, a solution containing 87 mM NaCl, 25 mM NaHCO$_3$, 10 mM glucose, 75 mM sucrose, 2.5 mM KCl, 1.25 mM NaH$_2$PO$_4$, 0.5 mM CaCl$_2$, and 7 mM MgCl$_2$ was used (equilibrated with 95% O$_2$/5% CO$_2$ gas mixture). For experiments, the slices were superfused with physiological saline containing 125 mM NaCl, 25 mM NaHCO$_3$, 25 mM glucose, 2.5 mM KCl, 1.25 mM NaH$_2$PO$_4$, 2 mM CaCl$_2$, 1 mM MgCl$_2$ (95% O$_2$/5% CO$_2$).

Patch pipettes were pulled from borosilicate glass tubing (2.0 mm outer diameter, 1.0 mm inner diameter) and filled with a solution containing 125 mM Cs-Gluconate, 20 mM CsCl, 2 mM MgCl$_2$, 2 mM Na$_2$ATP, 10 mM EGTA, 10 mM HEPES and 5 mM QX-314 (pH adjusted to 7.3 with KOH); pipette resistance was 5-7 MΩ. GFP-labeled 4-week-old adult-born neurons in the inner granule cell layer of hippocampus were identified with Zeiss LSM-700 confocal microscope. The stimulation pipette was filled with HEPES-buffered external solution and positioned at the inner half of the molecular layer. Both stimulation pipette and the patch pipette were positioned using Luigs & Neumann micromanipulators. Biphasic stimulation pulses (±60 μA, 200 μs) were generated via WPI A395current simulator and postsynaptic currents were recorded with an Axopatch 700B amplifier (Molecular Devices, Sunnyvale, CA). Series resistance (Rs) was below 50 MΩ with an average of 25.6 ± 2.2 MΩ

(n=9) in WT mice, not significantly different from recordings in dnSNARE mice (29.6 ± 2.6 MΩ, n=9, P = 0.29), and compensated by about 80%. Data were filtered at 10 kHz and 6 kHz for evoked EPSCs and mEPSC (internal four-pole low-pass Bessel filter), respectively, and sampled at 20 kHz using a 1401 power interface (Cambridge Electronic Design, Cambridge, UK). For display purpose, data were passed through an additional 1kHz low-pass Gaussian filter. For mEPSC analysis, data were further filtered at 500 Hz. Pulse sequences were generated using FPulse (University of Freiburg, Germany) running under Igor (version 5.01; WaveMetrics, Lake Oswego, OR) on a personal computer. To isolate excitatory postsynaptic responses, 100 µM Picrotoxin (Sigma) was added to the bath solution. To assess the effect of D-serine on synaptic NMDAr currents, 50µM D-serine was added in bath solution. For mEPSC recordings, in addition to picrotoxin, 0.5µM Tetrodotoxin (TTX) was added in physiological saline to block spontaneous action potential firing in slices. Recordings were made at 25 ± 2°C.

Data were analyzed with either self-written programs run in Wolfram Mathematica 10 or Stimfit 0.14 (https://github.com/neurodroid/stimfit). mEPSCs were analyzed as previously described (Schmidt-Salzmann et al., 2014). In brief, a template-matching algorithm was used implemented in Stimfit. First, a template was generated by fitting an exponential rise and decay to a synaptic waveform obtained from averaging large mEPSCs. In a second event-detection step, the template was slid over the recorded current trace and scaled to fit all the mEPSCs. As a selection criterion, the scaling factor was larger than 4-6 times the calculated standard error. False positive events were manually deleted. The remaining events were fitted with an exponential rise and decay. Statistical analysis were performed in GraphPad Prism 5.

In vivo microdialysis:
Mice were anaesthetized with isoflurane and were placed in a stereotaxic frame using a mouse adaptor (Kopf) with modified ear bars. Microdialysis probes were implanted in the DG (Bregma: -2 mm anteroposterior, 1.75 mm lateral and -2 mm dorsoventral). The active dialysis surface length of the cellulose membrane (concentric design, molecular weight cut-off 50 kDa) was 1 mm. The probe was secured in place with dental cement on the skull. Microdialysis experiments started 24 h after surgery. Ringer solution (125 mM NaCl, 2.5 mM KCl, 1.26 mM CaCl2, 1.18 mM MgCl2, 0.20 mM NaH2PO4) was perfused through the microdialysis probe at a flow of 1.0 µl/min using a high precision pump (CMA 400 syringe pump, CMA Sweden). Experiments were performed during the light period and mice were tested in their home cage. After at least a 2 h equilibration period, the dialysates were

collected every 30 minutes in small eppendorf tubes and directly frozen in liquid nitrogen and stored at -80°C until analysis. At the end of the experiment, animals were euthanized with an overdose of anesthetic and brains were removed and stored in 4% paraformaldehyde prior to histological confirmation of probe.

Astrocytic Culture and conditioned medium:

Astrocyte primary culture were purified from postnatal day 2-3 mice (dnSNARE or WT littermate animals). Hippocampus were mechanically triturated for homogenization and seeded onto 25 cm^2 flasks in Dulbecco's Modified Eagle Medium (DMEM) glutamax (Invitrogen, USA), 15% normal calf serum with penicillin/streptomycin (Invitrogen, USA). Cells were grown for 10 days in a humidified 5% CO2 incubator at 37∘C. At confluence, flasks were shaken at 230 rpm on an orbital shaker for 2 h to separate microglia from astrocytes and were washed with HBSS (Invitrogen, USA). Cells were then split and plated on 6 wells plate to generate pure astrocytic cultures. The enrichment of astrocytes in cultures was assessed by immunostaining. 98% of the cells expressed GFAP and none of the cells expressed the neuronal markers NeuN, DCX, TUJ1 or Map2 (data not shown), indicating that this procedure efficiently eliminates neurons.

After reaching confluence, culture medium was washed with HBSS (Invitrogen, USA) to eliminate residual serum, and replaced by saline buffer solution (500µl of Tyrode's solution : NaCl, KCl, CaCl2, MgCl2, HEPES and Glucose) for two hours. Astrocytic conditioned solution (ACS) was then collected, centrifuged (10 min at 1800 RPM) and filtered (0.22 um filter, Millipore) to remove cellular debris and immediately frozen at -80°c until HPLC analysis. Astrocytes were then washed with HBSS, separated using trypsin (Invitrogen), collected, centrifuged and immediately frozen for Bradford protein assay.

D-serine, Glycine, Glutamate and GABA extracellular concentration measurements:

The extracellular levels of D-serine, Glycine, Glutamate and GABA were then analyzed in dnSNARE mice, WT mice and WT and dnSNARE mice treated with D-Serine/NaCl, with a commercial laser-induced fluorescence capillary electrophoresis (CE-LIF) (CE: Beckman Coulter, P/ACE MDQ; LIF: Picometrics, LIF-UV-02, 410 nm 20 mW) as follows: The samples were processed for micellar CE-LIF and were fluorescently derivatized at RT for 60 min with napthalene-2,3-dicarboxaldehyde (NDA) before being analyzed by CE using a hydroxypropyl-β-cyclodextrin (HP-β-CD) based chiral separation buffer (Fossat et al., 2012). All electropherograms data were collected and analyzed using Karat 32 software v8.0

(Beckman Coulter, Fullerton, CA, USA). The quantity of neurotransmitters in the samples was determined from a standardized curve while peak identification was made by spiking the fraction with the corresponding amino acid. These analysis were performed by the Plateforme de Chimie Analytique (INSERM U862, University of Bordeaux, France).

Total internal reflection fluorescence microscopy

Astrocytes were plated on glass coverslips coated with 0.1mg/ml poly-D-Lysine (Sigma) at a density of $3x10^4$ cells per plate.

Images acquisition was performed as previously described (Bezzi et al., 2004). Briefly, coverslips were mounted in an experimental chamber at 37 °C (Harvard Apparatus) on the stage of a Zeiss Axiovert 200 fluorescence inverted microscope modified to allow epifluorescence (EPI) and evanescence field (TIRF) illumination (Visitron System). GFP$^+$ cells were identified with epifluorescence illumination (488 nm, xenon arc lamp, Visichrome polychromator system, Visitron), stained with 5 μM acridine orange (Molecular Probes) for 15 min at 37 °C in the dark and then washed. Cells were stimulated with ionomycin application at a final concentration of 1 μM. and imaged with TIRF illumination (488 nm laser, Visitron). Light entered the coverslips and underwent total internal reflection at the glass-cell interface. In our experimental conditions, penetration depth of TIRF illumination was calculated to be of about 90 nm. (Toomre, 2012). Light was filtered with a beam splitter (Zeiss filter set 10). Pixel size: 126 nm at binning 2. Video images, digitized with MetaFluor, were analyzed with MetaMorph software (Universal Imaging, USA). The fusion of acridine orange spots (flashes) in the whole-astrocytes were manually counted in bins of 10 sec, by designing a region of interest around the perimeter of the cell surface (160 000 pixels : 85 μm2) in the TIRF field. Acridine orange flashes were characterized by an increase (over 4 fold of the basal level) a spread and then decline of fluorescence. Although there has been reports of artifacts using TRF imaging (Brunstein et al., 2014a; Brunstein et al., 2014b) this technique is widely used to compare vesicular release in similar samples.

Supplemental References

Bezzi, P., Gundersen, V., Galbete, J.L., Seifert, G., Steinhauser, C., Pilati, E., and Volterra, A. (2004). Astrocytes contain a vesicular compartment that is competent for regulated exocytosis of glutamate. Nature neuroscience 7, 613-620.

Brunstein, M., Herault, K., and Oheim, M. (2014a). Eliminating unwanted far-field excitation in objective-type TIRF. Part II. combined evanescent-wave excitation and supercritical-angle fluorescence detection improves optical sectioning. Biophys J 106, 1044-1056.

Brunstein, M., Teremetz, M., Herault, K., Tourain, C., and Oheim, M. (2014b). Eliminating unwanted far-field excitation in objective-type TIRF. Part I. identifying sources of nonevanescent excitation light. Biophys J 106, 1020-1032.

Fellin, T., Halassa, M.M., Terunuma, M., Succol, F., Takano, H., Frank, M., Moss, S.J., and Haydon, P.G. (2009). Endogenous nonneuronal modulators of synaptic transmission control cortical slow oscillations in vivo. Proc Natl Acad Sci U S A 106, 15037-15042.

Fossat, P., Turpin, F.R., Sacchi, S., Dulong, J., Shi, T., Rivet, J.M., Sweedler, J.V., Pollegioni, L., Millan, M.J., Oliet, S.H., and Mothet, J.P. (2012). Glial D-serine gates NMDA receptors at excitatory synapses in prefrontal cortex. Cerebral cortex 22, 595-606.

Halassa, M.M., Florian, C., Fellin, T., Munoz, J.R., Lee, S.Y., Abel, T., Haydon, P.G., and Frank, M.G. (2009). Astrocytic modulation of sleep homeostasis and cognitive consequences of sleep loss. Neuron 61, 213-219.

Nolte, C., Matyash, M., Pivneva, T., Schipke, C.G., Ohlemeyer, C., Hanisch, U.K., Kirchhoff, F., and Kettenmann, H. (2001). GFAP promoter-controlled EGFP-expressing transgenic mice: a tool to visualize astrocytes and astrogliosis in living brain tissue. Glia 33, 72-86.

Pascual, O., Casper, K.B., Kubera, C., Zhang, J., Revilla-Sanchez, R., Sul, J.Y., Takano, H., Moss, S.J., McCarthy, K., and Haydon, P.G. (2005). Astrocytic purinergic signaling coordinates synaptic networks. Science 310, 113-116.

Schmidt-Salzmann, C., Li, L., and Bischofberger, J. (2014). Functional properties of extrasynaptic AMPA and NMDA receptors during postnatal hippocampal neurogenesis. J Physiol 592, 125-140.

Slezak, M., Grosche, A., Niemiec, A., Tanimoto, N., Pannicke, T., Munch, T.A., Crocker, B., Isope, P., Hartig, W., Beck, S.C., et al. (2012). Relevance of exocytotic glutamate release from retinal glia. Neuron 74, 504-516.

Sterio, D.C. (1984). The unbiased estimation of number and sizes of arbitrary particles using the disector. Journal of microscopy 134, 127-136.

Sultan, S., Gebara, E., and Toni, N. (2013). Doxycycline increases neurogenesis and reduces microglia in the adult hippocampus. Front Neurosci 7, 131.

Tashiro, A., Makino, H., and Gage, F.H. (2007). Experience-specific functional modification of the dentate gyrus through adult neurogenesis: a critical period during an immature stage. The Journal of neuroscience : the official journal of the Society for Neuroscience 27, 3252-3259.

Thuret, S., Toni, N., Aigner, S., Yeo, G.W., and Gage, F.H. (2009). Hippocampus-dependent learning is associated with adult neurogenesis in MRL/MpJ mice. Hippocampus 19, 658-669.

Toni, N., Teng, E.M., Bushong, E.A., Aimone, J.B., Zhao, C., Consiglio, A., van Praag, H., Martone, M.E., Ellisman, M.H., and Gage, F.H. (2007). Synapse formation on neurons born in the adult hippocampus. Nature neuroscience 10, 727-734.

Toomre, D. (2012). Alignment and calibration of total internal reflection fluorescence microscopy systems. Cold Spring Harb Protoc 2012, 504-509.

Zhao, C., Teng, E.M., Summers, R.G., Jr., Ming, G.L., and Gage, F.H. (2006). Distinct morphological stages of dentate granule neuron maturation in the adult mouse hippocampus. The Journal of neuroscience : the official journal of the Society for Neuroscience 26, 3-11.